Costa Rica Institute of Technology

University of Groningen

Academic Area of Mechatronics Engineering

Faculty of Science and Engineering

Positioning control and port-Hamiltonian based model for compound eyes microscopy.

Graduation Project Report to opt for the Licentiate degree of Mechatronics Engineer.

Oscar Fonseca Aguilar
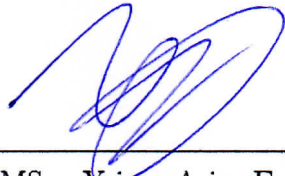
Cartago, March 18, 2019

Declaration of Authorship

I declare that the graduation project is entirely made by myself, with the help of the cited literature, my own and the different scientists and engineers knowledge from University of Groningen and the Costa Rica Institute of Technology. Therefore, I assume total responsibility for the work done and the content of the final report.

<div style="text-align: right">

Oscar Fonseca Aguilar

Groningen, March 18, 2019

ID: 3-0488-0402

</div>

Instituto Tecnológico de Costa Rica
Área Académica Ingeniería Mecatrónica
Proyecto de Graduación
Tribunal Evaluador

Proyecto de Graduación defendido ante el presente Tribunal Evaluador como requisito para optar por el título de Ingeniero en Mecatrónica con el grado académico de Licenciatura, del Instituto Tecnológico de Costa Rica.
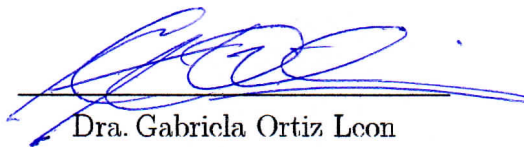
Miembros del Tribunal

_____
MSc. Yeiner Arias Esquivel
Profesor Lector

_____
Ing.Paula Monge
Profesora Lectora

_____
Dra. Gabriela Ortiz Leon
Profesora Asesora

Los miembros de este Tribunal dan fe de que el presente trabajo de graduación ha sido aprobado y cumple con las normas establecidas por el Área Académica Ingeniería Mecatrónica.

Cartago, 08 de marzo del 2019

Instituto Tecnológico de Costa Rica

Área Académica Ingeniería Mecatrónica

Proyecto de Graduación

Tribunal Evaluador

Acta de Evaluación

Proyecto de Graduación defendido ante el presente Tribunal Evaluador como requisito para optar por el título de Ingeniero en Mecatrónica con el grado académico de Licenciatura, del Instituto Tecnológico de Costa Rica.

Estudiante: Oscar Enrique Fonseca Aguilar

Nombre del Proyecto: *Positioning control and port-Hamiltonian based model for compound eyes microscopy.*

Miembros del Tribunal

_____   _____

Profesor Lector   Profesora Lectora

_____

Profesora Asesora

Los miembros de este Tribunal dan fe de que el presente trabajo de graduación ha sido aprobado y cumple con las normas establecidas por el Área Académica Ingeniería Mecatrónica.

Nota final del Proyecto de Graduación: _____

Cartago, 08 de marzo del 2019

Resumen

El aparato goniométrico robótico para ojos compuestos (GRACE) de la Universidad de Groningen requiere un sistema de posicionamiento preciso para el uso de un telemicroscopio con el objetivo de analizar los ojos compuestos de insectos y su caracterización. En esta tesis el lector puede obtener información sobre la creación de este sistema, el cual incluye el diseño del circuito, identificación del sistema, creación de la interfaz grafica y diseño del control del motor CD facilitado para esta tarea.

Palabras clave: GRACE, sistemas port-Hamiltonianos, position. palabras, clave, ...

Abstract

The Goniometric Robotic Apparatus for Compound Eyes (GRACE) at the University of Groningen requires a precise positioning system to use a telemicroscope with the goal of analyzing and characterizing the compound eyes of insects. In this thesis the reader can obtain information regarding the creation of this system, this includes the circuit design, the system identification, the graphic user interface, and the control design for the DC motor given to accomplish this task.

Keywords: GRACE, port-Hamiltonian systems, position.

Dedicated to my parents for always encouraging me to follow the desires of my heart, for forever being an example of good values, and giving me the support to experience this unique opportunity.

To my siblings for taking care of me and giving me advice every time I needed.

To my grandparents for their love and lessons of hard work.

To all the people who has taught me a valuable thing and helped me through this wonderful journey that is life.

Acknowledgements

Contents

List of Figures

List of Tables

Table 1: Description of Symbols Used.

Symbol	Name	Units	Value
i_a	Armature Current	A	NA
q_m	Rotational Position	count	NA
k_m	Torque Constant	$\frac{Nm}{A}$	NA
k_b	Back EMF Constant	$\frac{Vs}{rad}$	NA
p	Screw's Pitch	$\frac{mm}{rev}$	6
d_m	Screw's Medium Diameter	mm	12
c	Counts to distance converter	$\frac{\mu m}{count}$	1.55
P_R	Lifting Load Required Force	N	NA
P_L	Lowering Load Required Force	N	NA
λ	Inclination Angle of Screw Threat	rad	$\frac{p}{\pi d_m}$
f	Friction Coefficient Aluminum-Steel		0.6
N_s	Number of Teeth on Sun Gear		16
N_p	Number of Teeth on Planet Gears		11
N_c	Number of Teeth on Crown		41
N_i	Number of Teeth on the gear between encoder and screw		18
N_{enc}	Number of Teeth on Encoder's Gear		9
N_s	Number of Teeth on Screw Gear		34
$\theta_{m,enc,t}$	Speed of motor's shaft, encoder, screw	$\frac{count}{s}$	NA
$T_{m,enc,t}$	Motor, Encoder and Screw's Torque	N m	NA
r	Counts per revolution on the encoder		1024

Nomenclature

Abbreviations

AC	Alternating Current
CPP	Corneal Pseudo Pupil
DC	Direct Current
DOF	Degrees of Freedom
DPP	Deep Pseudo Pupil
FBD	Free Body Diagram
GRACE	Goniometric Robotic Apparatus for Compound Eyes
GUI	Graphic User Interface
HMI	Human Machine Interface
IC	Integrated Circuit
LED	Light Emitting Diode
LTI	Linear Time Invariant
PBC	Passivity Based Control
PC	Personal Computer
PDE	Partial Differential Equation
pH	port-Hamiltonian
PID	Proportional Integral Derivative
PWM	Pulse Width Modulation
SPI	Serial Peripheral Interface
SSE	Stable State Error

Chapter 1

Introduction

1.1   Main Motivation

Natural phenomena have proven to be a great source of inspiration for developing special-ized devices. In the Department of Computational Physics at the University of Groningen the ongoing studies on insect compound eyes have driven the development of a device called GRACE: a Goniometer Robotic Apparatus for Compound Eyes shown in Figure 1.1.
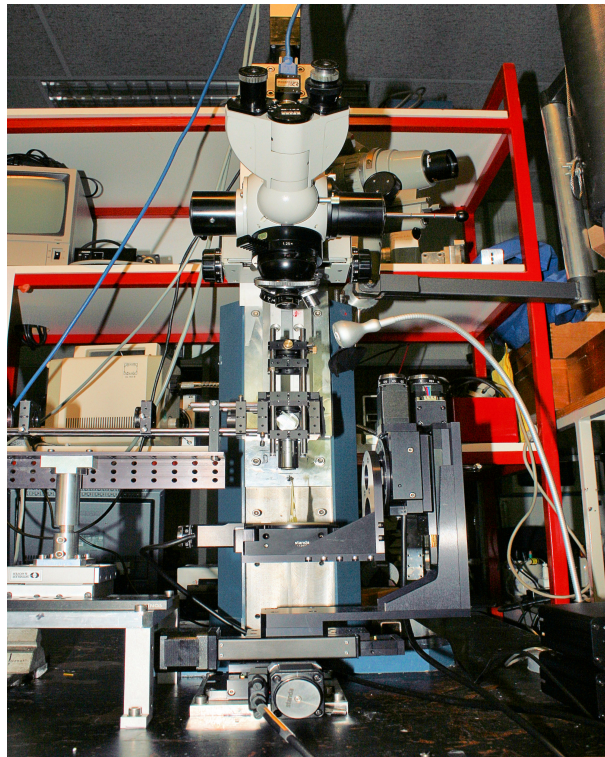
Figure 1.1: Last version of GRACE

The device above has been evolving, product of the collaboration of different scientists and engineers since the first mechanical implementation in [1] to the last contribution by [2] and [3], consisting in an auto focusing and auto centering algorithms to the improve the quality of the image. The above by automatically looking for the sharpest focus point and centering the insects eye. As part of the optimization of the project, the necessity of a nonlinear positioning control system for a DC motor, which moves a microscope, became apparent. In [4] the first attempt to create this controller was done, but the design was not based on the motor used in GRACE, and the connection with the Matlab was not developed, originating several issues with the implementation. The aim of the project described in the present document is to develop and install the required highly accurate control system for the GRACE. The last, to work with insects with different physiology and come up with more accurate models to represent the insect's eyes than the already existing, obtained by manual methods.

1.2   State of the Art

The computational physics laboratory, have focused efforts in studying the eyes of arthropods such as butterflies, and the GRACE project is the result of the need of a faster, more accurate and systematic way to analyze compound eyes are.

The first steps to create such a machine are present in [5], by creating an optical arrange that allows the study of more complex characteristics on the compound eye. Later, during the resent years, several projects involving the improvement of GRACE have taken place, regarding the mechanical issues, in [6] a 6 degrees of freedom (DOF) system using Arduino was developed. Then, a feedback on the angular position of the system was implemented by [7]. Using Matlab, improvements on the image quality were done in [8], [2] and [3] by creating filtering, auto focusing and auto centering algorithms respectively. In [4], an attempt of a position control for the telemicroscope axis can be seen, nonetheless, the objective was not achieved due non considerations in the model, communication and the systems logic. The aforementioned, leads to the development of a new logic and communication suitable for all cases present on the system, as well as a consideration for the new controller explained in the present thesis.

1.3   Main Contribution

The implementation of the motor control system is intended to allow a precise study of the field of view of the ommatidium, and of the interommatidial angles (angles between the region of view of one ommatidium respect to another [9]), by using the pseudo pupil (PP) phenomenon. Figure 1.2 shows the arrangement of the apparatus, with the motor in the M axis, which is to be controlled by the actuator.
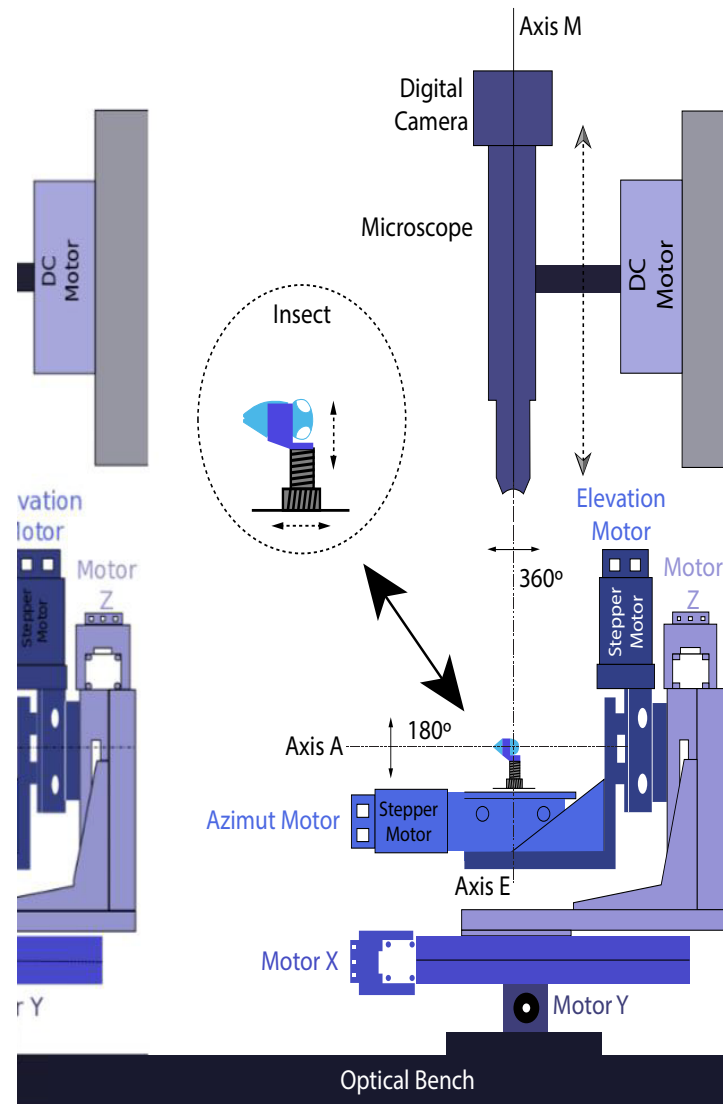
Figure 1.2: GRACE 2 axis configuration, where the DC motor in the M axis moves the telemicroscope, the X,Y,Z,E,A axes are moved by stepper motors, being the last two moved in a rotational framework, all combined for the insect to be placed in any position desired, and the image to be focused as needed, taken from [3].

By accomplishing this project and using GRACE, the accuracy of 5 μm on the M axis will allow to make a detailed map of the compound eyes of insects which cannot be studied before due the complications their physiology gave to the focus system actuated by the Z-axis showed in Figure 1.2. Furthermore, the distribution of the interommatidial angles is possible using the divergence of the light at different focal levels, allowing studies as the one presented in Figure 1.3, realized in the late 70s, by using trigonometry to calculate the actual angles.
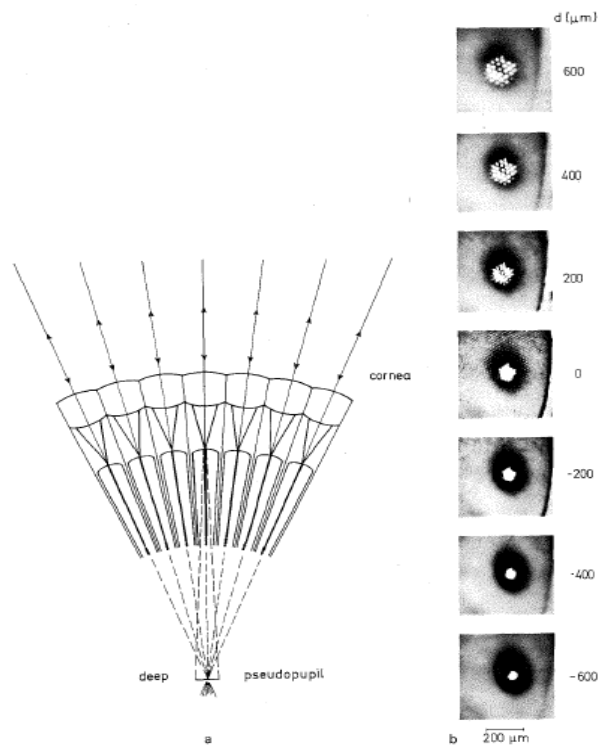
Figure 1.3: Compound eyes seen on steps of 200 μm apart [9], gradually showing the separation
between the light emitted by the ommatidia and with calculation the actual value
of the interommatidial angles can be obtained.

The success of this research is the first step to a more accurate model of the eyes of arthro-
pods [2], and in a future, leading to new advances in vision systems who can correctly
reproduce the behavior of compound eye not accomplished by previous models, [10], [11].

1.4   Objectives and documents structure

The main objective of the project is the design and implementation of a control algorithm
for the telemicroscope axis of the GRACE system, considering it's non-linearities. The
process consist on the design of a controller circuit adequate for the actual system but also
giving the possibility for the system to grow in functionalities, the final control system is
compared to a preliminary PID controller to ensure the improvement regarding a linear
control theory. Once the system is validated the new feature is incorporated to the GUI
for the user to overview the GRACE using the PC. Using the aforementioned statements,
the objectives can be written as the following.

1.4.1   General Objective

- Develop an automatic control for the M axis of the GRACE system by considering non-conservative forces to enhance the accuracy and fasten the mapping of compound eyes.

1.4.2   Specific Objectives

- Evaluate the components and control method needed in GRACE 2 considering the system necessities and capabilities.

- Design and test a PID controller for the system incorporating different filtering methods to have a framework of the possible improvements for GRACE.

- Design a nonlinear automatic control, that considers the selected variables and forces acting in the movement and positioning of the motor.

- Integrate the PID control system to all the other algorithms used in the operation of GRACE 2 by programming the controller to run the control developed.

1.4.3   Document Structure

The present document is divided in 7 section including the current. In Chapter 2 all the theory to develop and understand the system is presented. Furthermore, Chapter 3 explains the process used to get to a solution for every objective. Moreover Chapter 4 shows the design in terms of hardware, software and the process to characterize the system and it's controller. In addition to this, Chapter 5 display and analyze the results. Last, conclusions and recommendations are given in chapters 6 and 7.

Chapter 2

Theorical Basis

The chapter introduces the concepts employed in the project, stated by previous authors. The main purpose is for the reader to have the knowledge needed to comprehend the reason and the flow of developed solution. In the first part a brief explanation of the compound vision is done, to understand the complexity of the subject and how the GRACE helps to study them. Next, the maths involving the optics on GRACE, which play a role on the final state of the solution, are developed. Following, control engineering approaches are introduced with their pros and cons. Finally the non-linear control law is explained from scratch starting from the physics in which is based, and ending with the specific solution used.

2.1   Compound Vision

The compound vision is a growing field of study due the possibilities it can give to develop new technologies. The specific study of butterflies and flies vision is the purpose of the GRACE project. The compound eye is conformed by thousands of visual structures called ommatidium, which arrangement gives the animal capabilities as, focusing, high light adaptation, specialized vision areas, and a wide range of vision [9]. Using each ommatidium, the insects brain stitch every piece of visual information into the full image. The structure itself holds certain properties of interest for the GRACE, in the 2.1 the diagram of the compound eye is shown.
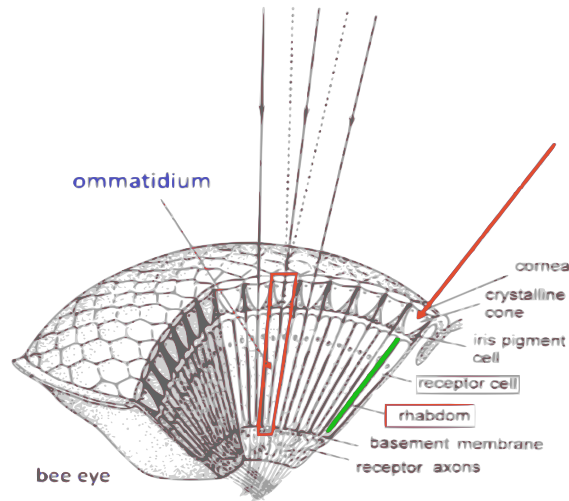
Figure 2.1: Bee Apposition Compound Eye [2], the rhabdom (photosensitive component of the ommatidia) is marked in green, an omatidium is outlined in red. Moreover, the black lines denote the vector of the outgoing light of the eye forming interomatidial angles between them. Each component of the basic structure is named an marked in its respective position.

The black arrows indicate the visual axes of adjacent ommatidia, the angles between the visual axes are called interommatidial angles, and together with the characterization of the different pigments, and the region of view of the ommatidia are, the main properties studied in the University of Groningen. Each ommatidium is capped by a facet lens, and a crystalline cone (marked by the red arrow), which focus incident light onto the rhabdom, transporting the wave to the light-sensitive sense cells, where the light is traduced into an electrical signal. Figure 2.2 presents a detail of an ommatidium marking all the relevant and noticeable parts.
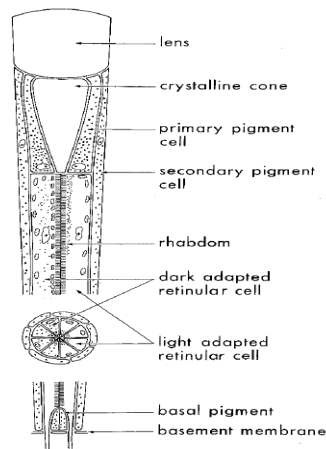
Figure 2.2: Diagram of an ommatidium of a butterfly compound eye [2], where the primary and secondary pigment cells marked function, is to screen and transform the light into electrical signals, for specialized functions such as matting or hunting [12]. The dark and light adapted retinula helps the insect to adapt its vision to the available light, while the basal trachea serves as a tapetum.

Because insects live in different environments, and have different behaviors, the eye is not necessarily uniform, meaning that the size and shape of the ommatidia can vary depending on the region of the eye is being studied [12], [13]. The use of incident light onto the eye, reveals the optical phenomenon called pseudo pupil (PP) which consist in the light reflected into the tapetum (mirror at the back of the eye, serves to increase the light available). The above is used to observe the change in the nature of each ommatidium [3], [12].

2.2   Optical Apparatus

In Figure 2.3, a diagram of the optical arrangements employed to observe the PP of the insect is shown. The light source is collimated by L_1, while D_1 is the far field diaphragm used to control the amount of incoming light from the source. Later, the light is focused by the intermediate lens L_2, into the near-field diaphragm D_2. The last mentioned, dictates the area of the eye illuminated, being D_2 in the focal plane of the first telescope lens L_3. Then, the light ray is directed to a lens L_3 situated at 45°, using a half-mirror M placed to make both axes confocal. Furthermore, L_4 then focus the light into the CPP at the back of the insects eye, finally, the telescope pair of L_4 and L_5, image the CPP into the back focal plane of L_5. There the last diaphragm D_3 is placed [3]. For another configuration implemented to study the arthropods eyes see [5].
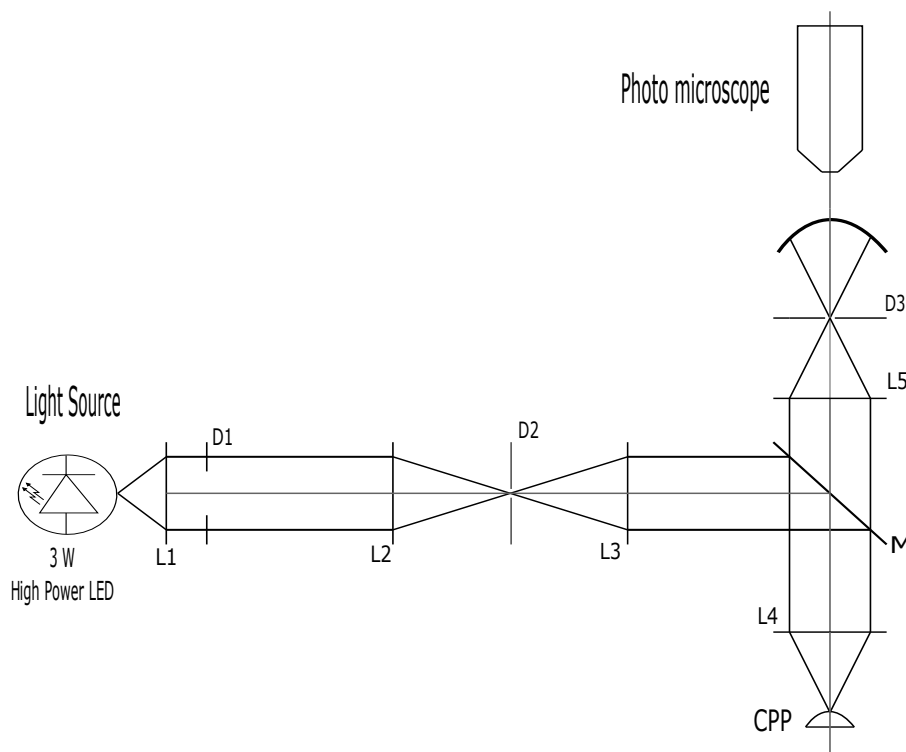
Figure 2.3: Schematic diagram of the optical arrangement used to insect eye photography, being the light source a 3 W high power LED with dimming capacity, for more information see [14].

2.2.1   Magnification

The current section explains the functioning of the optics, however, the values of the lens affect the size of the image seen by the microscope. Figure 2.4 shows a more detailed diagram of the telescope (vertical axis) in the optical apparatus.
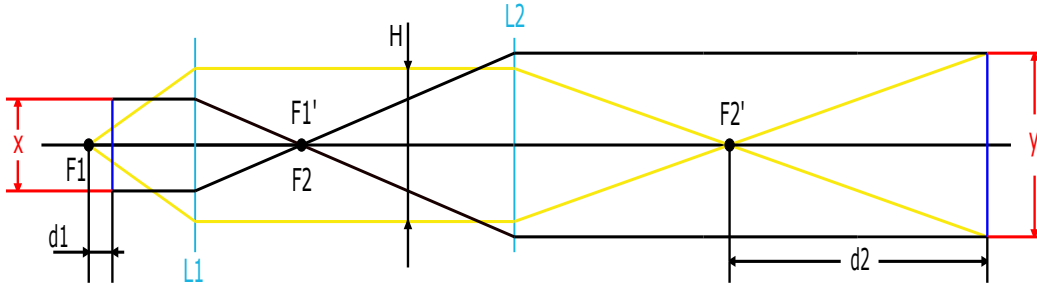
Figure 2.4: Telescope arrangement placed in the vertical axis of the GRACE optical apparatus. Where F1 is the focal point of the first lens, F2 is the focal point of the lens L2. H, x, y, d1, d2 stand for the height of the collimated light ray coming from F1, the size of the object, size of the image, distance of the object from the focal point F1 and distance of the image from F2 respectively.

The optics presents a lateral magnification, stating x and y as the size of the object and the image respectively, the mathematical relation of their sizes is,

$$\frac{y}{x} = \frac{f_2}{f_1}, \tag{2.1}$$

additionally, the arrangement presents another magnification factor explained by (2.2),

$$\frac{x}{d_1} = \frac{H}{f_1}, \qquad \frac{y}{d_2} = \frac{H}{f_2},$$
$$\frac{x f_1}{d_1} = \frac{y f_2}{d_2}, \tag{2.2}$$
$$\frac{d_2}{d_1} = \frac{y f_2}{x f_1} = \frac{f_2^{\,2}}{f_1^{\,2}},$$

with d_1 and d_2 the distances in the longitudinal axis, knowing the values of f_1 and f_2 showed in Table 1, a magnification of 25X from one end to the other is concluded, meaning that a movement in the microscope side of the optics is perceived as a displacement 25 times smaller for the eye mapping.

2.3   DC Motor Simplified Model

A DC motor is a basic use actuator in control engineering that transforms voltage into a rotating or linear motion, with the help of a coupling for the second. The torque generated

by a motor is proportional to the current through it:

$$T = K_t i, \tag{2.3}$$

The movement in the motor backlashes to the electrical system as the back-electromagnetic force, which is proportional to the current speed as,

$$V_{bemf} = K_e \dot{\theta}, \tag{2.4}$$

assuming a viscous friction b on the motor's shaft, and using Kirchhoff's and Newton's law the state equations can be derived:

$$J\ddot{\theta} + b\dot{\theta} = K_t i, \tag{2.5}$$

where J is the systems rotational inertia, and θ is the angular position, therefore its derivates respect to time correspond to angular velocity and acceleration.

$$L\frac{di}{dt} + Ri = V - K_e \dot{\theta}, \tag{2.6}$$

with L, R, i, V being the inductor value (H), the value of the resistor (Ω), the current (A) and the input voltage (V) of the circuit, respectively.

To obtain the transfer function of the motor, first is necessary to apply the Laplace transform to (2.5) and (2.6). Then, assuming the velocity as output and the voltage as input, and finally assuming $K_t = K_e = K$. (2.7) is the result,

$$\frac{\dot{\theta}(s)}{V(s)} = \frac{K}{(Js + b)(Ls + R) + K^2} \tag{2.7}$$

The expression can then be simplified by multiplying and dividing the transfer function with the value of R and assuming $\frac{L}{R} << 1$ to eliminate one pole of the model transforming it into:

$$\frac{\dot{\theta}(s)}{V(s)} = \frac{\dfrac{K}{R}}{(Js + b) + \dfrac{K^2}{R}} \tag{2.8}$$

2.4 Control Theory

2.4.1 PID

The PID controllers are the most common feedback controller in the industry, and consists of three basic coefficients, proportional, integral and derivative [15]. Each coefficient work with the error calculated, and intend to solve an inconvenient in the system response, to then join the three into a full control signal. The error can be calculated either by subtracting the set point to the current state or the other way around, resulting into a direct or reverse control. There are two main PID forms, the parallel and the ideal, shown in the Figure 2.5 respectively.
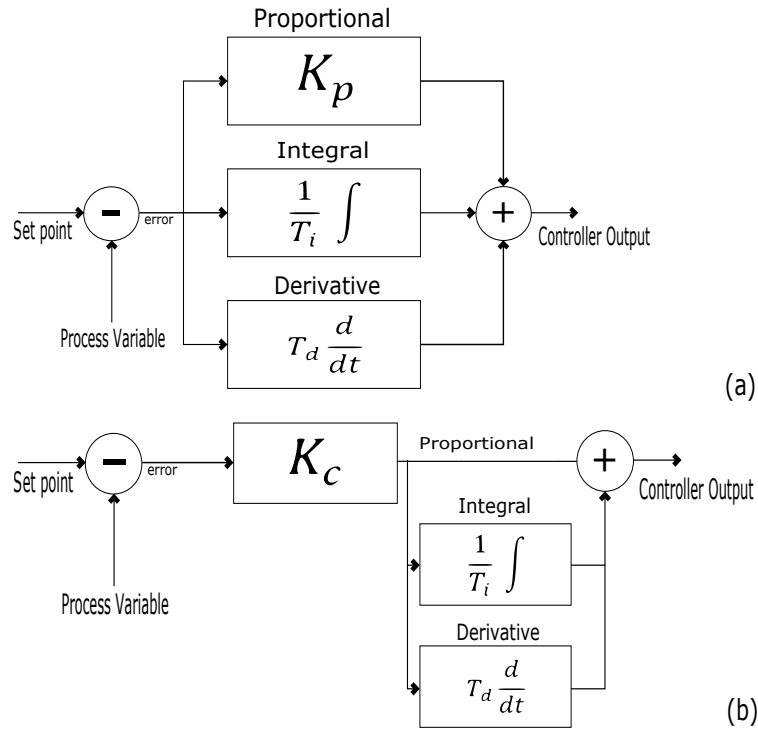
Figure 2.5: System diagram of parallel and ideal PID controllers, (a) and (b) respectively, [15].

The first, is designed in a way that all terms are independent one from another, with their own gains as shown in (2.9), while the ideal is intended to have a controller gain K_c which at the same time is the same value as the proportional gain, being all three part of the controller in terms of the proportional resulting in the expression in (2.10).

$$C(t) = K_p e + \frac{1}{T_i} \int e \, dt + T_d \frac{de}{dt}, \tag{2.9}$$

$$C(t) = K_c \left(e + \frac{1}{T_i} \int e \, dt + T_d \frac{de}{dt} \right). \tag{2.10}$$

2.4.1.1 Proportional

The proportional's function is to augment or decrease the scale of an action done by an actuator according to the actual difference between the current state and the desired. When increased the gain has effects on the speed of the systems response, nonetheless going to a value to high might cause oscillations. The proportional gain is the only one of the three that can be used alone as a simple controller, being sometimes enough for the system's requirements [16], since this gain doesn't always guarantees a zero state error.

2.4.1.2 Integral

The integrator, is responsible of reduce the difference between the desired and the actual behavior of the system, stable state error. The above is done by accumulating the values of the system's error over time and multiplying the resulting by the integral gain to make the sign of the error significant for the control [17].

2.4.1.3 Derivative

Finally, the derivative oversees enhancing the speed of the system response. The previous is done by looking at the change of the system's state respect to time, and counteracting the action according to the rate computed when the system is close to the set point to avoid overshoot.

2.4.1.4 PID Tuning

Nowadays, there are lots of tuning methods for the gains of a PID, such as Ziegler-Nichols methods, damped oscillation, internal model control, and Fertick method to name a few [18]. However, most of the methods used need certain conditions to be achieved to start the design or tuning process, for the cases these requirement aren't meet, the empirical tuning is needed, by knowing the action of each value the values are changed until a desired response is achieved. In the following subsections, the first two mentioned methods are explained giving three different ways of tuning the controller [19].

2.4.1.5 Ziegler-Nichols First method

The method consist in obtaining the system's response to the unit step, resulting in a signal shaped as Figure 2.6. Using the inflection point in the curve to draw a tangent line, the stable value delay (L) and the time (T) constants can be obtained by graphical methods. Using L and T, and assuming a parallel configuration the values of the PID

gains will follow the Table 2.1.
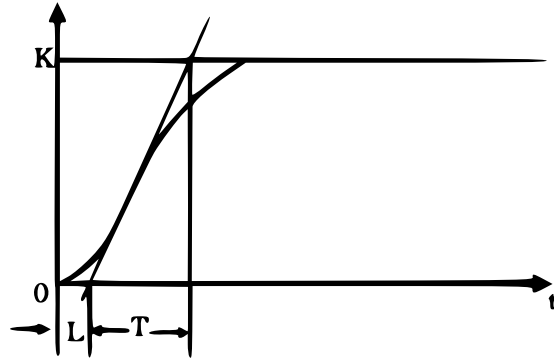
Figure 2.6: Step response for tuning the PID with the Ziegler-Nichols first method. L is the delay value and T refers to the time constant, taken from [19].

Table 2.1: Ziegler-Nichols first method rule

Control Type	K_p	T_i	T_d
P	$\dfrac{T}{L}$	∞	0
PI	$0.9\dfrac{T}{L}$	$\dfrac{L}{0.3}$	0
PID	$1.2\dfrac{T}{L}$	$2L$	$0.5L$

2.4.1.6   Ziegler-Nichols Second Method

Is somehow similar to an empirical tuning, the system needs to be in a closed loop, where the proportional gain can be manipulated. The goal is to find a gain K_{cr} that provokes the system to go into an oscillation behavior, as the signal in Figure 2.7. Then, using the critical gain and the period, the values of the PID are as stated in Table 2.2, it's important to say that, the method is only possible if the system owns a critical gain.
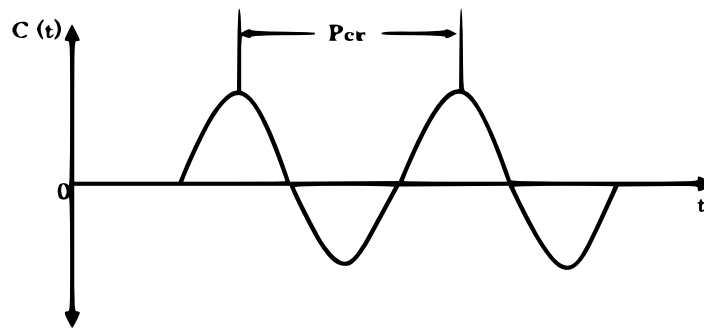
Figure 2.7: Sustained oscillation obtained with a proportional feedback, and used to obtain the PID values by the Ziegler-Nichols second method. P_{cr} refers to the period of the signal, taken from [19].

Table 2.2: Ziegler-Nichols second method rule

Control Type	K_p	T_i	T_d
P	$0.5K_{cr}$	∞	0
PI	$0.45K_{cr}$	$\dfrac{P_c r}{1.2}$	0
PID	$0.6K_{cr}$	$0.5P_{cr}$	$0.125P_{cr}$

2.4.1.7 Damped Oscillation Method

There are cases where using a closed loop with a proportional gain doesn't gives the sustained oscillations seen in Figure 2.7, and the open loop test of 2.6 can't be succeeded. Damped oscillation, goes for a k_d in the proportional controller such that the system the behavior of the Figure 2.8, [20].
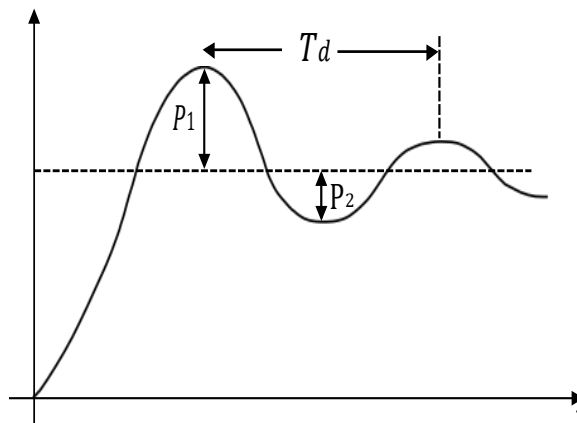
Figure 2.8: Damped Oscillation Method with its values of importance.

The objective value is when the damping presented in (2.11),

$$\frac{P_2}{P_1} = \frac{1}{4},$$

(2.11)

and by measuring the value of the damped period T_d, the (2.12) statements have to be followed.

$$k_p = k_d, \quad \tau_i = \frac{T_d}{6}, \quad \tau_d = \frac{T_d}{1.5}$$

(2.12)

2.4.2   Passivity Based Control

Dissipativity is a property of certain systems, which is related to the energy dissipation. In terms of control systems (inputs and outputs), the energy introduced to the system $u(t) \in \mathbb{R}^n$ is greater or equal to the stored in it, being the difference between them the dissipated energy [21]. The passive systems are a restrictive case of the dissipative in which the flow of the incoming energy to the system is stated by $u^T y$ (with $y \in \mathbb{R}^m$ as the output). Passivity can be used to express non-linear systems as long as they are TI and have relative degree not greater than one [22]. Passive systems hold an invariability property, meaning that the interconnection of two or more passive systems remains passive, combining the aforementioned advantages allows an easier modeling of complicated systems, using Euler-Lagrange or Hamiltonian energy frameworks.

The passivity based control aim is to reach a passivity closed-loop system for achieving the system stability. In general terms, the control is based in two stages, first an energy shaping of the system in which commonly is applied to the potential energy of the model using the close-loop to generate a "new" desired potential energy having a global and single minimum at the equilibrium point. Second, a damping injection modifying the original damping of the system, ensuring the asymptotically stability of it, is important to declare that neither of the stages have an standard method to obtain the new expressions for the energy or damping. Besides the lack of a systematic procedure, passivity is used for set point control and tracking problems on fully and under actuated systems.

2.5   Hamiltonian Energy Framework

To introduce the framework in subject, a recall from basic physics is needed, where a Lagrangian system is expressed as,

$$\frac{d}{dt}\left(\frac{\partial L}{\partial q_i}\right) - \frac{\partial L}{\partial q_i} \qquad i = 1, ..., n$$

(2.13)

where the Lagrangian is defined by [23],

$$L = T\left(t\right) - V\left(t\right) = \frac{1}{2}m\dot{q}^2 - V\left(t\right); \tag{2.14}$$

here q_i is the position on the coordinate i of the system, T(t) and V(t) the kinetic and potential energy respectively , resulting the formulation into a second order differential equation (DE) of n variables. Moreover, the Hamiltonian dynamic equations are defined by (2.15)

$$
\begin{aligned}
\frac{dq_i}{dt} &= \frac{\partial H}{\partial p_i} \\
\frac{dp_i}{dt} &= \frac{-\partial H}{\partial q_i}
\end{aligned}
\tag{2.15}
$$

being q_i the coordinates, and p_i the conjugate momenta of the system defined as $p_i = m\dot{q}_i$, and H the Hamiltonian, which plays a role analog to the force for Newtonian or the Lagrangian in Lagrange mechanics. The Hamiltonian approach can be described in terms of Lagrange as seen in (2.16) and (2.17), by using two fundamental variables instead of one, the model turns into a first order differential equation with 2n variables.

$$p_i = \frac{\partial L}{\partial \dot{q}_i}, \tag{2.16}$$

$$H\left(q, p\right) = \sum_i \dot{q}_i p_i - L. \tag{2.17}$$

The change of order respect from Lagrangian is widely used to model non-linear systems and perform stability analysis [24].

2.6   Port-Hamiltonian Systems

The pH framework is a energy based approach on the systems modeling, their interconnection structures, and power ports [25]. By connecting different subsystems expressed in terms of energy, a wide spectrum of (non linear) systems can be described including mechanical, electrical hydraulic and thermal systems. The network modeling is mainly used for dividing complex problems into simpler models which are described by the energy elements, the dissipation elements and the power preserving ports [25], based on the Dirac structures [26]. The general expression for a pH system, introduced by [27], is,

$$
\Sigma = \begin{cases}
\dot{x} = \left[J\left(x\right) - R\left(x\right)\right]\dfrac{\partial H\left(x\right)}{\partial x} + g\left(x\right)w \\
y = g\left(x\right)^T \dfrac{\partial H\left(x\right)}{\partial x}.
\end{cases}
\tag{2.18}
$$

with $x \in R^N$ being the states of the system, $J(x) \in \mathbb{R}^{N \times N}$ an interconnection matrix, which by definition needs to have the skew symmetry property, $R(x) \in \mathbb{R}^{N \times N}$ a semi-definite positive damping matrix, and $H(x) \in \mathbb{R}^N$ the Hamiltonian. The last term in the space state is composed by the matrix $g(x) \in \mathbb{R}^{N \times M}$ responsible of changing the value of the input $w \in \mathbb{R}^M$ and by consequence the equation $y \in \mathbb{R}^M$. Where $N \geqslant M$ representing fully and under actuated systems when $N = M$ or $N > M$ respectively. Narrowing to a more specific case, lets present a standard n-dimensional mechanical system with the addition of an external force, described by,

$$\begin{bmatrix} \dot{q} \\ \dot{p} \end{bmatrix} = \begin{bmatrix} 0_{nxn} & I_{nxn} \\ -I_{nxn} & -D(q,p) \end{bmatrix} \begin{bmatrix} \dfrac{\partial H(q,p)}{\partial q} \\ \dfrac{\partial H(q,p)}{\partial p} \end{bmatrix} + \begin{bmatrix} 0_{nxn} \\ G(q) \end{bmatrix} u + \begin{bmatrix} 0_{nxn} \\ B(q) \end{bmatrix} e_f. \tag{2.19}$$

The mechanical case in (2.19) is called forced port-Hamiltonian systems, since apart from the control input an external force e_f is acting on it. Here q and p refers to the position and the momenta respectively, using them as states the system can be expressed in terms of potential and kinetic energy considering variable mass, as this last one is included on the p state.

2.6.1   Control with only position measurements

Section 2.4.2 introduced the creation of a new potential energy and damping injection as control strategies for energy based models. In [28], the energy shaping control using both potential and kinetic energy is shown, the above using Euler-Lagrange systems. The work done in [29] proves that damping injection can be done by a dynamic extension making unnecessary the use of velocity measurements for potential energy shaping. Assuming a conservative mechanical port-Hamiltonian, $R(x) = 0$,

$$\dot{x} = J(x) \frac{\partial H(x)}{\partial x} + g(x) u$$
$$y = g(x)^T \frac{\partial H(x)}{\partial x}, \tag{2.20}$$

it's Hamiltonian is defined as in (2.21), with $M(q)$ being the mass matrix of the system:

$$H(q,p) = \frac{1}{2} p^T M(q)^{-1} p + V(q) \tag{2.21}$$

The goal as a PBC is to obtain a new desired energy, this is accomplished by modifying the interconnection to be $J_d(x)$ and in the case of (2.20) the incorporation of a damping matrix $R_d(x)$.

$$\dot{x} = [J_d(x) - R_d(x)]\frac{\partial H_d(x)}{\partial x} \tag{2.22}$$

$J_d(x)$ is then written in terms of the desired mass (if the system does not change it's mass $M_d = M$) and another skew symmetric matrix $J_2(x)$ of choice, as seen in (2.23).

$$J_d = \begin{bmatrix} 0 & M(q)^{-1} M_d(q) \\ -M_d(q)^{-1} M(q) & J_2(x), \end{bmatrix} \tag{2.23}$$

where $R_d(x) \geqslant 0$ keeping the bounding from bellow property. The desired Hamiltonian to adjust the system for a set point q^* is,

$$H_d(q,p) = \frac{1}{2} p^T M_d(q)^{-1} p + V_d(q). \tag{2.24}$$

Using both Hamiltonians result into the matching conditions equation [30]:

$$g(x)^\perp \left[(J_d(x) - R_d(x)) \frac{\partial H_d(x)}{\partial x} - J(x) \frac{\partial H(x)}{\partial x} \right] = 0 \tag{2.25}$$

being $g^\perp g = 0$. The signal of the controller can be decomposed into two terms regarding the energy shaping and the damping injection,

$$u_{es}(q,p) = \left(g(x)^T g(x) \right)^{-1} g(x)^T \left[J_d(x) \frac{\partial H_d(x)}{\partial x} - J(x) \frac{\partial H(x)}{\partial x} \right], \tag{2.26}$$

$$u_{di} = -R_d(x) g(x)^T \frac{\partial H_d(x)}{\partial x}. \tag{2.27}$$

By interconnecting the controller and the system using the Hamiltonian instead of the ports, the resulting system is expressed by:

$$\begin{bmatrix} \dot{x} \\ \dot{x}_c \end{bmatrix} = \begin{bmatrix} J_d(x) & 0 \\ 0 & J_c(x_c) - R_c \end{bmatrix} \begin{bmatrix} \dfrac{\partial \overline{H}_d}{\partial x} \\ \dfrac{\partial \overline{H}_d}{\partial x_c} \end{bmatrix} \tag{2.28}$$

being $x_c = [q_c, p_c]^T$ and defining M_c as the controller's mass, the new Hamiltonian is,

$$\overline{H}_d(q,p,q_c,p_c) = \frac{1}{2} p^T M_d(q)^{-1} p + \frac{1}{2} p_c^T M_c(q_c)^{-1} p_c + \overline{V}_d(q,q_c), \tag{2.29}$$

recalling (2.25) the new matching conditions presented in [26] are described by (**??**)

$$G(x)^\perp \left[\frac{\partial V}{\partial q}(q) - M_d(q) M(q)^{-1} \frac{\partial \overline{V}_d}{\partial q}(q,q_c) \right] = 0 \tag{2.30}$$

it doesn't matter the way the system is interconnected since both $\overline{V}_d(q, q_c)$ and $V_d(q)$ are fixed by $V(q)$. In [31] the systems able to asymptotically stabilize by dynamical extension are:

- Systems that need only potential energy shaping such as fully actuated.

- Systems with constant mass.

In the first case, the non consideration of kinetic energy shaping eliminates the use of velocity measurements, while in the second by having a constant mass the kinetic partial DE (PDE) disappears. Besides the matching condition, for the closed loop with the extension to work, the resulting system needs to have a minimum Hamiltonian with q and q_c constant, and for the derivative of new potential energy respect to the controller state to be zero at q_c on it's minimum both explained in (2.31) and (2.32) respectively.

$$\frac{\partial \overline{H}_d(q, q_c)}{\partial q} = 0 \qquad q = q^*, q_c = q_c^*. \tag{2.31}$$

$$\frac{\partial \overline{V}_d}{\partial q_c} = 0, \tag{2.32}$$

where q^* and q_c^* can be changed to modify the minimum of the Hamiltonian [21]. As stated before, the kinetic energy is not necessary to stabilize the system, even though, the transient response is affected by it. The dynamic extension incorporate a dynamic not involving the speed of any the system nor the extension, the controller dynamic for enhancing the response is explained by the interconnection and damping matrices:

$$J_c = 0$$
$$R_c = \begin{bmatrix} \overline{R}_c^- 1 & 0 \\ 0 & 0 \end{bmatrix}, \tag{2.33}$$

Finally obtaining the expression for the state of the controller (2.34):

$$\dot{q}_c = -\overline{R}_c^- 1 \frac{\partial \overline{V}_d(q, q_c)}{\partial q_c} \tag{2.34}$$

Chapter 3

Materials and Methods

In the present thesis the work developed follows a process divided by aspects to improve, regarding hardware, software, system functioning. Each change in the above three represent a review on the other two, to ensure a good synergy between all the parts of the GRACE, transforming the process in an iterative flow [32]. To initiate the design a bibliographic review and a preliminary request by the final user is done, to then start the iterations needed as shown in Figure 3.1.
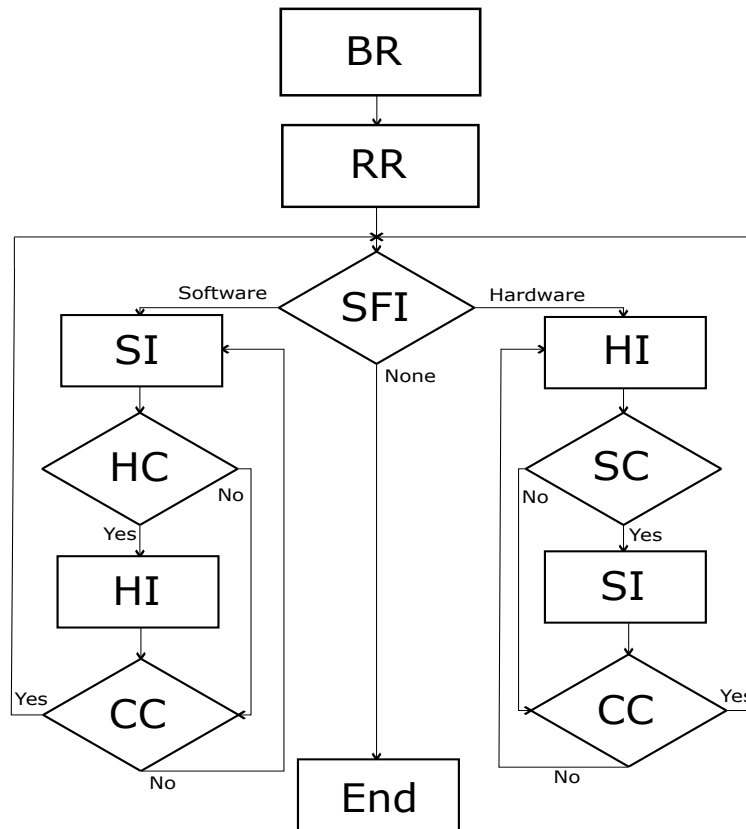
Figure 3.1: Work flow for process takne in the present thesis.

BR, RR, SFI, SI, HC, HI, SC, CC stand for bibliographic review, request review, system

function improvement, software improvement, hardware change, hardware improvement, software change and change check respectively.

Every betterment needs the approval of the laboratory team to be effective, creating more runs to the process depending on the decision taken collectively. The whole product is targeted to users not familiar with engineering concepts making the feedback from the computational physics department relevant for the design [33]. The objectives of the thesis don't follow a hardware or software solution only, making the division stated at the beginning of this chapter the most logical to understand each part of the final product, nonetheless the methodology objective wise is stated in the rest of the chapter.

3.1 Evaluating the components and control methods for GRACE 2

The circuit design is established by modifying the work done in [4], consisting in a LED and motor controller. The components to analyze for improving the circuit are, the micro controller display (besides having a GUI, the system requires having a manual mode were you can work without the PC), the current limiter and the security system for the motor ends. Additionally, the circuit is modified to not include unnecessary elements and incorporate missing components after the previously mentioned changes. The control law used for the design is selected by taking the access to it's knowledge, noise sensibility, factors involved and computing resources used into consideration, being the first one the more significant of all. A table with the proposed paradigms and their their evaluation is generated, for the laboratory team to choose among them.

3.2 Design and test a PID controller for the system

The design of the PID comes together with the system functioning, several steps are taken before creating the controller including sensor characterization, noise elimination, friction consideration. The values of the constant of the controller are tuned experimentally using the knowledge about how each one of them affect the system's behavior, and considering the construction of the controlled motor to avoid undesirable phenomenons. The test of the developed control is done going up and down considering that the system acts differently depending its direction, furthermore, a verification of the system real position value is made using a mechanical sensor to validate the measurement done for the set point.

3.3 Design a non-linear automatic control

Using the selected controller among the proposed, a model that fits the framework of the law selected is developed by considering the mechanical phenomena present in the motor. A control is designed following the corresponding rules for the selected law, additionally, a simulation of the system is done considering an ideal power source, in order to prove the systems convergence to the desired point and tell whether the action of the circuit used is affecting significantly to the motor or not.

3.4 Integrating the control system to all other algorithms used in GRACE by programming the micro-controller

By using the feedback of the lab partners and considering that the M-axis needs both a manual and an automatic mode, the program is created using Arduino and Matlab as stated in previous works done in the system [3], [6]. Tests are performed to accomplish the user requirements, and ensure the full integration of GRACE. The last is done by adding the use of the DC motor to the already existing graphical user interface and creating a communication method for it to send commands to the micro-controller.

Chapter 4

System Design

The control of the M-axis position is a challenge that needed to be boarded through different approaches, first a hardware properly designed for the handling of all the subsystems is mandatory. Second, the logic to change between different operation modes and a graphic user interface to oversee the state are required. Third, a system identification process is necessary in order to know how to create the controller. Last, the controller needs to be designed knowing the system's values and limits, all the aforementioned is explained in the following sections.

4.1 Hardware Selection

The system is composed by 7 main parts, the power supply, motor control, the DC motor, micro-controller (Arduino Mega), sensor, the LED controller and the display. The overall system is connected to a PC using the USB port of the Arduino as in the diagram of Figure 4.1.
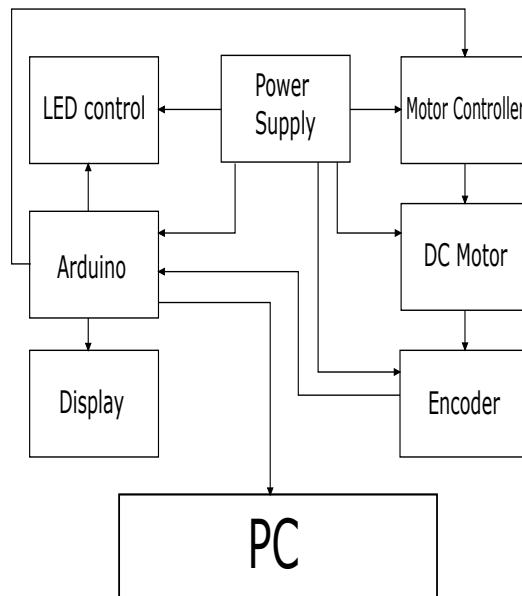
Figure 4.1: Controller circuit block diagram.

The design is a modification of the circuit in [4], where the objective is to improve all the possible aspects, such as consumption, pin-out designation, human-machine interface, security of the system. The above leads to the an analysis of specific components changed or added, explained in the following subsections, and by consequence the elimination of certain parts such as the cooling fan and the Arduino Nano.

4.1.1   Display

The system uses a touchscreen as HMI, allowing the user to interact with the system using the screen only, however, it requires an extra Arduino Nano to sync with the main Arduino Mega, and the graphics need to be updated (via SD card) when the setup is. Since the Mega is not using all it's pins, having an Arduino Nano is not an optimal solution, the HMI shows the state of a LED and the motor position. There are certain requirements for the new display to meet, first, the screen needs enough space to inform the user about the working mode of the illumination and positioning systems. Second, the minimum amount of pins used is the optimal in order to keep the Arduino dedicated pins available for further work. Finally, the communication with the system needs to be fast enough to update the values of the encoder, the Table 4.1 shows a summary of the necessities to be fulfilled.

Table 4.1: Wanted features for the display

Feature	Value
Symbols	Alphanumeric
I/O pins	Minimum possible
Rows	4
Columns	16
Frequency	150 kHz

Considering all five criteria, the I2C 2004 [34] display is selected, the decision is based mainly on the display communication protocol (I2C, eliminating the need of the Arduino Nano) and the available space of 4 rows and 20 columns. Althought, the selected screen doesn't interact with the user as the touchscreen does, the previous HMI was used only for selecting the operation modes of the main subsystems, which with the LCD is going to be done via switches.

4.1.2   Current Limiter

An Arduino can't manage a DC motor due the power necessities, for helping the micro controller the L298N DC motor driver is added to the circuit. Besides the mentioned, a new issue is created in the system, being the driver's current capacity 2 A, and having the motor a higher inrush current than 2 A. To solve the current problematic, instead of

changing for a high power driver, a more convenient solution is to sacrifice the motor's torque and place a current limiter in between the L298N and the motor. The circuit for limiting the current used in [4], consist in a well known and proven solution, despite that, the space occupied by this circuit was more than the wanted and limitation caused heating on the components. To apply proved circuit without generating noticeable heat, a LT1083 voltage limiter in feedback is chosen, solving this way the heating problem. Having the new limiter a voltage dissipation of 1.2 V only, the heat generated by the power dissipation is not concerning anymore, leading to the decision of eliminating the cooling fan previously used.

4.1.3 Protection circuit

The positioning is done using a linear actuator Elero Junior 1, which features can be seen in [35], the machine consists on a motor connected to a lead screw. Being a DC motor, the rotation of the motor itself is not constrained, however the rotation is bounded by the lead screw ends. If not stopped when the ends are reached, the DC motor would try to keep running, becoming apparent the need of a security measure. The aforementioned consist in, the anti-bouncing integrated circuit MC14490 which specifications can be observed in [36], to prevent false values from the end switches, due the fact of the last ones are mechanical parts. Then the circuit is followed by a resistor arrangement, the reason of the hardware approach to the present problem is because gives a more reliable security than a software based solution.

4.1.4 DC-DC converters

In circuit manufactured in [4], the source of the components is powered using the 5 V output of the Arduino. Even though, there is nothing that forbids the use of that pin to power other low voltage elements, the solely power supply of the Arduino is not optimal for a system is prone to become larger. Therefore, two components are added to the circuit, the Traco TEL-3-2412 and the Traco TEL-3-2411 [37].The first one consist in a 24 V to 12 V DC-DC converter use to power the micro controller and available for adding any other 12 V component. While the second is a 24 V to 5 V DC-Dc converter used directly as a substitute for the 5 V output of the Arduino as the source to all the remaining elements.

4.2 Software

GRACE is an evolving mechatronic system existing before the development of the present thesis. Therefore, the software and firmware used in the automations and algorithms were

already settled before the beginning of the present project. The system uses complicated matrices calculation and image processing, hence, Matlab is the software used to compute and display the results, while communicating with the different controllers needed to perform the eye scan. The firmware of the telemicroscope control is handled with an Arduino MEGA capable of regulating the light source intensity going to the optical apparatus and movement of the motor, and yet powerful enough to have extra I/O available in case of needing new features in the coming future.

4.2.1   Arduino Communication and Control Algorithm

The Arduino needs to manage 5 main inputs, the PC communication, the sensor, the LED and motor potentiometers and mode selections. The system control 4 outputs as well, the LCD display, the serial protocol with the PC, finally, the LED and motor controllers. In Figure 4.2 a general flow chart of the desired script is shown, each block in the Figure is another subroutine to be explained in this section.
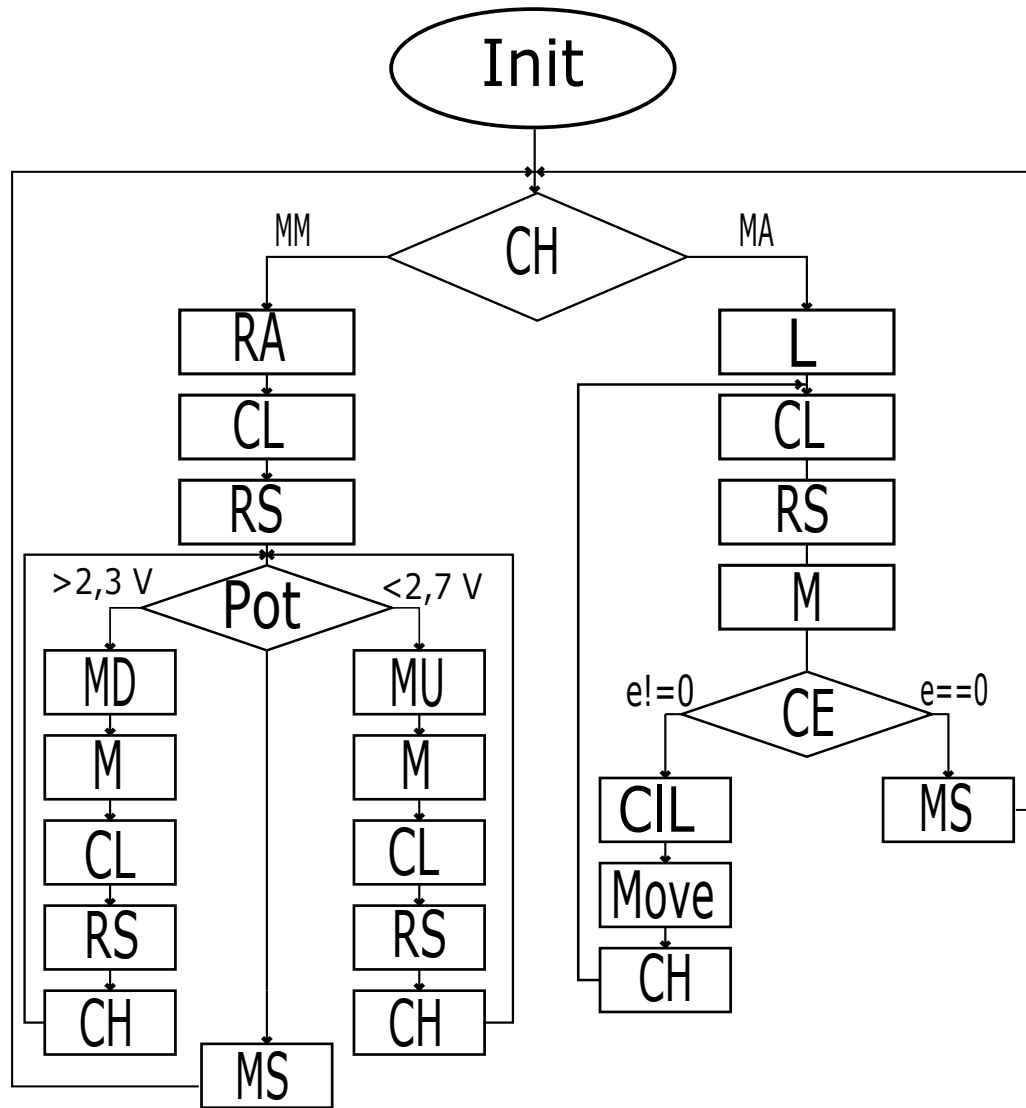
Figure 4.2: Process for the required script on the micro-controller.

In the Figure the names are simplified, with Init the initialization of the system, CH the subroutine to check the operating mode, MM and MA stand for motor manual and motor automatic. Furthermore, RA is the function to reset the automatic mode, CL is the process intended to control the LED, RS the steps needed to refresh the screen, Pot is the reading of the motor potentiometer, MD/MU refer to move down and move up. Additionally, L is for the asynchronous communication used to listen the PC, M is the measure of the system's state, CE the calculation of the error in the automatic mode, ClL is the control law for the automatic mode, and MS the motor stop.

The first step in the program is to initialize all the pins, variables and interrupts needed to manage the I/O. Second, the Arduino is in a constant loop checking the mode of the motor controller. If the manual mode is selected, the priority is to reset the values of the flags used in the automatic mode, preparing the system for the next time the automatic mode is activated, next the LED controller is called and later the screen is updated with the last data. Depending of the potentiometer value the motor stops, and goes back to

verify the state of the controller mode, or moves up/down while the position is measured, then the LED and the screen are called inside the second level loop to refresh the values even if the system is moving the motor. On the other side, when the automatic mode is activated, it starts by receiving commands from the PC. Later, calls the LED and screen to update values, finally it measures and calculate the error to whether apply a control law as the motor input or stop the motor and go back to check the system status. In the following subsections the subroutines of the script are explained, Figures mentioned are at the end of the section.

4.2.1.1   Check LED

The present function is similar to the general algorithm, it is called in every loop at different levels of the process to ensure that the LED will be controlled all time. It needs to decide whether the controller is on automatic or manual mode and read the respective input in charge of the control at that moment as shown in Figure 4.3.
CM standing for check operation mode, Pot referring to the reading of the potentiometer used for the manual mode, L to the listening routine for the data coming from the PC. ADC is for the conversion from the potentiometer to the digital value for the PWM and WL is used to short the analog write on the LED.

4.2.1.2   Check Mode

The function needs to read the switches used to change the LED and motor controllers mode and break the current mode of the one is changed if its necessary. A flowchart of the algorithm is presented in Figure 4.4.
In the Figure, RMS and RLS refer to the reading of the switch dedicated for the motor and the LED mode change respectively. Moreover, C? used as a verification to know if the respective mode has changed from the previous run. Finally BA and BM means a break on the automatic or manual mode respectively.

4.2.1.3   Refresh Screen

Due the fact that the display is an LCD screen, it is not necessary to keep refreshing all the characters in the screen, the subroutine just need to know what characters to refresh in order to have a smooth HMI. The Figure 4.5 shows the main logic of the function needed.
First, C? is the mode change verification, second, Cl meaning a clear in the display. Third, LM stands for denoting if the change was done in the LED or in the motor. Fourth LCD and MCD referring to the LED and motor change on the display respectively. Finally, RV being the refresh of the values written in the screen.

4.2.1.4 Move Up/Down

The two routines are triggered when a certain value is reached by the potentiometer, the algorithm needs to read the corresponding range of values of the resistor and map them into the corresponding range according to the permitted actuation in the required direction.

4.2.1.5 Listen

The function communicates with the PC when data is available in the serial port initiating and terminating the protocol by detecting specific characters. Then tells if is a command regarding the LED or the motor controller as in Figure 4.6. This process used in both automatic modes.

In the Figure, DA is marking the wait of the availability of the data, SR standing for the serial read of the incoming commands. R? is used to recall if the transmission is progress or not. Moreover, EC and SC stand for the ending and starting character of the protocol. SC is for saving the current symbol read. RT and RP, respectively mean the receiving is terminated or in progress. Dec is the subroutine for decoding the message received, LM is the conditional to modify whether the lightning or the position system. Finally, AM, W and SP, the first referring to the verification for the system to realize if it's on the correct mode, the second and third standing for analog write and the set point.
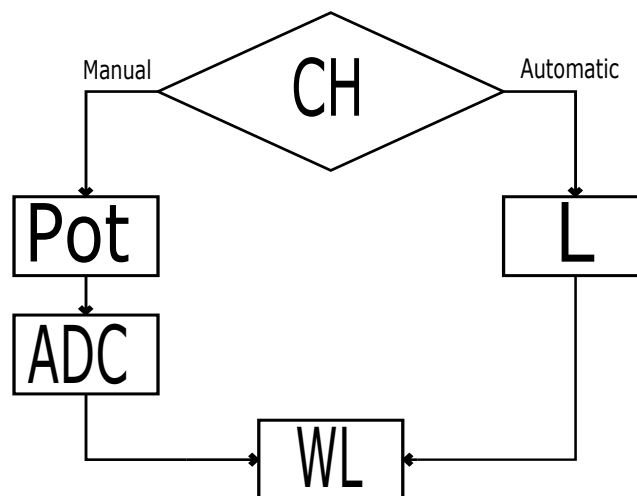
Figure 4.3: LED controller logic.
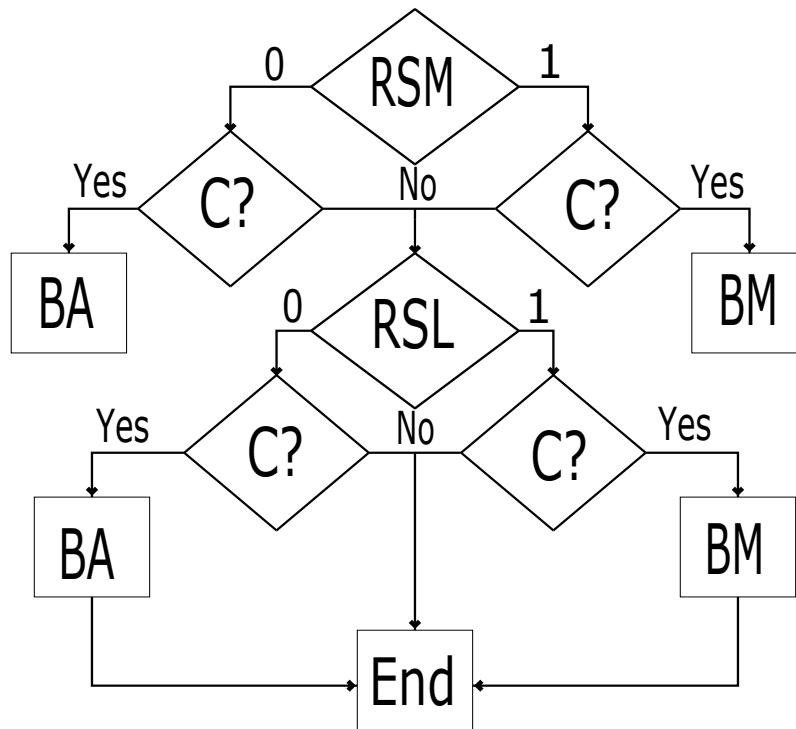
Figure 4.4: Automatic/Manual mode verifying process.
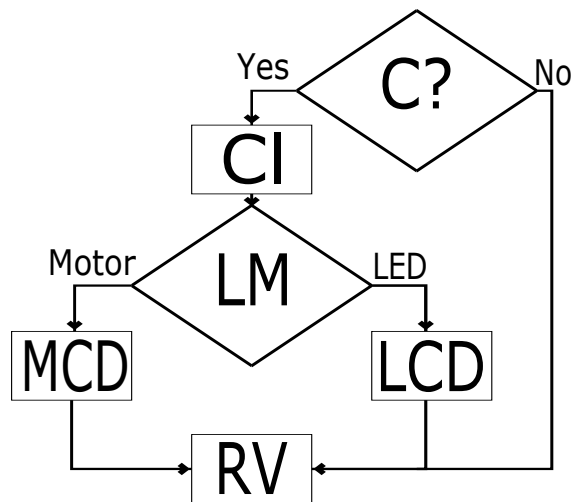
Figure 4.5: Optimized screen refresh process.
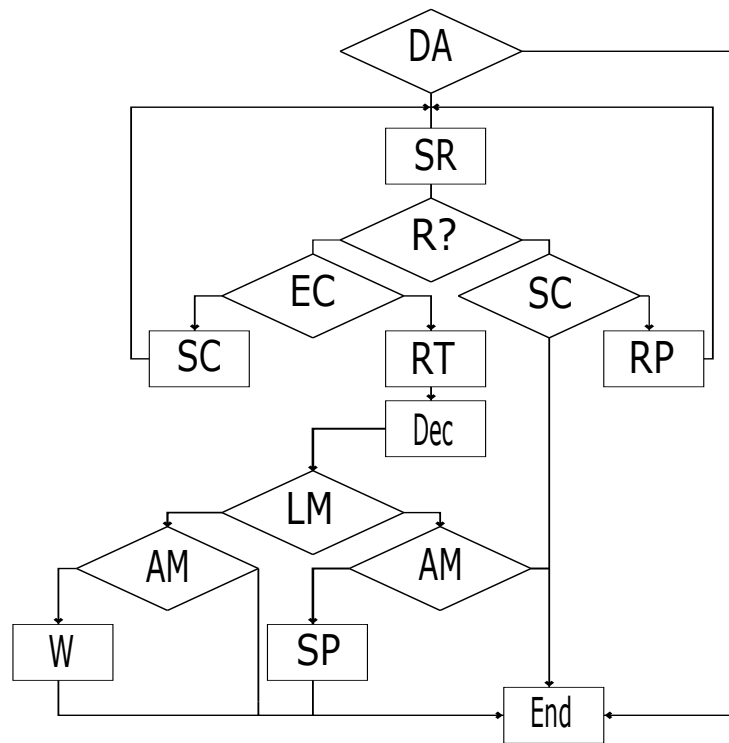
Figure 4.6: PC Data acquisition flow for the Arduino.

4.2.2 Graphic User Interface

Besides the telemicroscope position controller, the GRACE system also deals with another 5 DOF, actuated by Standa stepper motors [38]. The last mentioned get its inputs via Matlab GUI, created by [39] using dedicated libraries given by the manufacturer. In order to have a united system, the M axis controller needs to be included in the aforementioned GUI. Since the position's measurement is dictated by an asynchronous sensor as the optical encoder is, the communication with the circuit requires a protocol capable of receive and send information immediately after is available. In Figure 4.7 the logic of the GUI for the asynchronous communication is shown, the graphic user interface is not a running script in a loop waiting for the inputs to change as the system in an Arduino, taking that into consideration the panel dedicated to this purpose needs to wait for it's own buttons and the controller interruptions an trigger a specific script dedicated to each one of them.
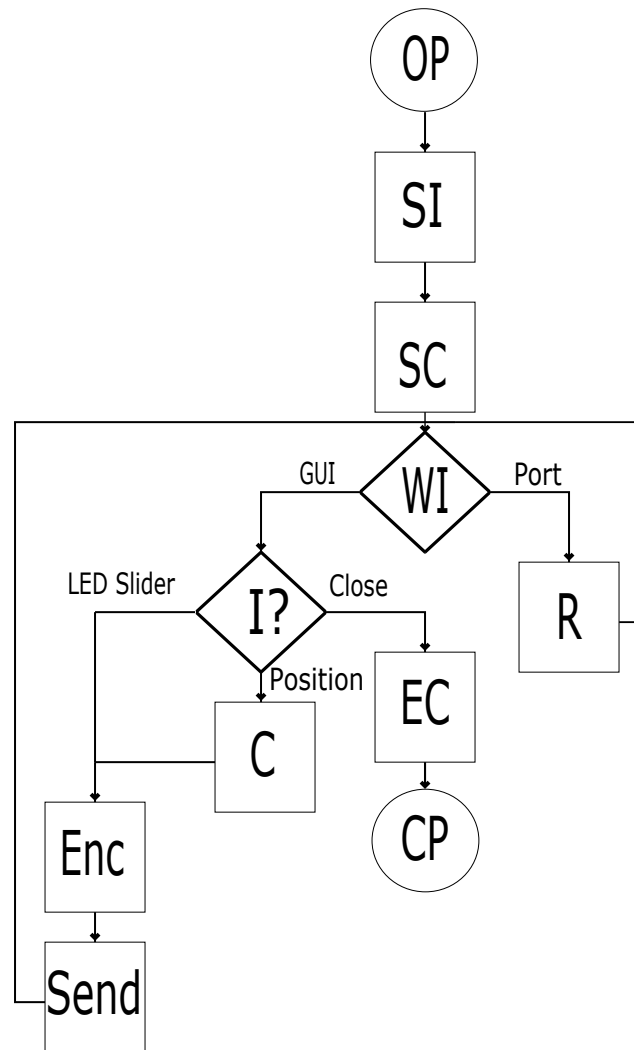
Figure 4.7: GUI needed process. OP, SI, SC, WI, R, I?, C, Enc, EC and CP stand for open
port, save port information, start communication, wait for interrupt, receive, in-
put type conditional, conversion, encode, end of communication and close port
respectively.

Besides the implications on the programming of the GUI, the controls need to offer a
understandable and user friendly display. The system state is showed by a non absolute
sensor, and is not operated by the developer of the control system, therefore, the controls
need to be explicit if the user is whether working with absolute coordinates or not.

4.3   System Controller

4.3.1   System Identification

The actuator internal mechanics and the encoder's resolution are aspects not specified
by the manufacturer. The obtainment of the above play an important role in the system

identification, the previous and the acquisition process for each is explained the following subsections.

4.3.1.1 Actuator Mechanics

The Elero Junior 1 is an actuator which traduce the rotation of a DC motor to linear motion, and the use of mechanical components to accomplish the transformation is evident. To obtain an accurate theoretical model of the system the values and setting of the mechanics, and the number part of the motor need to be known. Opening the device to check the values of the components, such as number of teeth for the gears, and the pitch of the screw is inevitable if the nonlinear controller is wanted to be accurate enough to have the desired performance. The Figures 4.8 and 4.9 show the values of the mechanic interconnections from the motor to the encoder and from the encoder to the rod respectively, both manually checked by disarming the actuator.

Gears P
N = 11

Gear S
N = 16

Gear C
N = 41
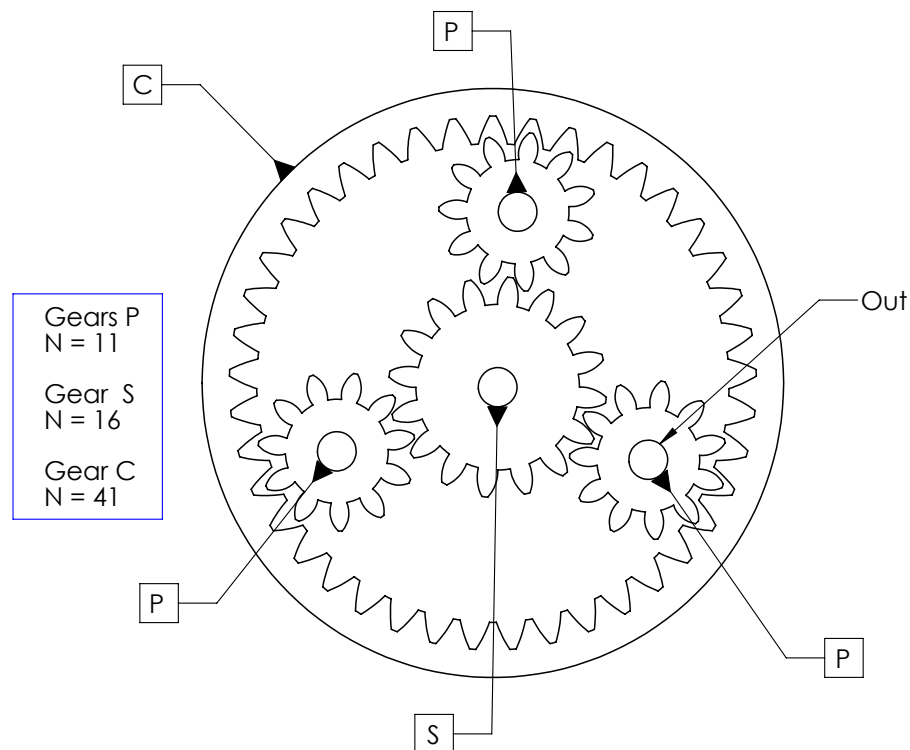
Figure 4.8: Gearing between the DC motor and the encoder with it's respective values, where the motor is connected on the sun gear G_s, and the encoder is attached to the three planetary gears G_p and being the crown of the system G_c part of the case, therefore, always in repose.
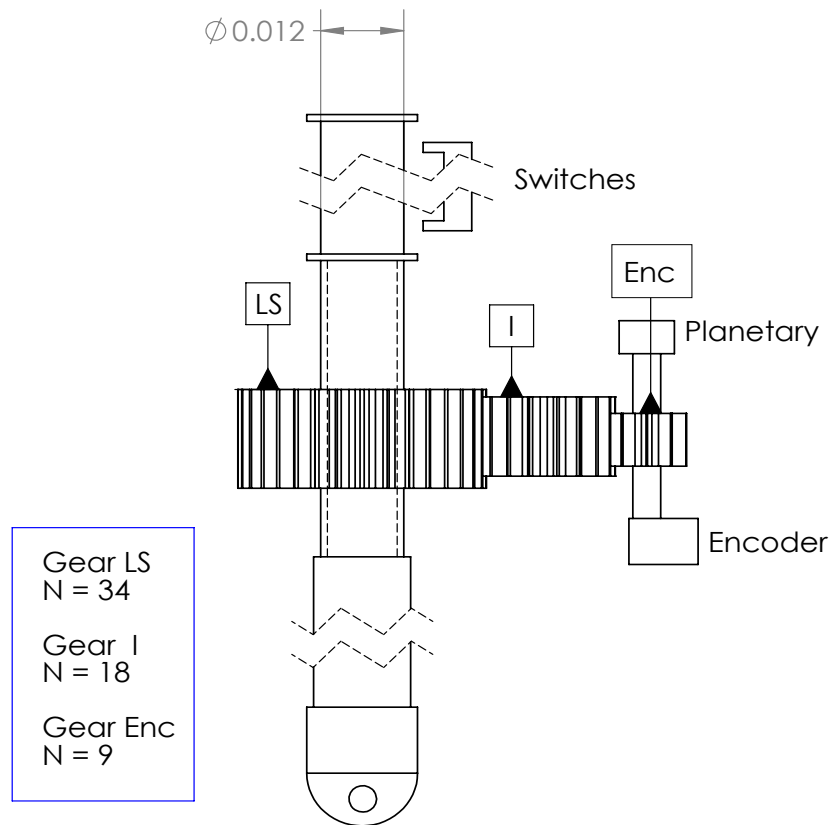
Figure 4.9: Connection between the encoder and the rod, being the screw's pitch 6 mm per revolution.

4.3.1.2 Encoder

An optical rotational encoder is a digital sensor which output is certain amount of pulses per each full turn. The sensor used in this case is not specified by the manufacturer and is not easily removable, additionally, the channel O (telling when a full turn is completed) is damaged, making its resolution impossible to find using an oscilloscope. For finding the sensor values another sensing device is needed, in Figure 4.10 a distance mechanical measuring tool is shown.
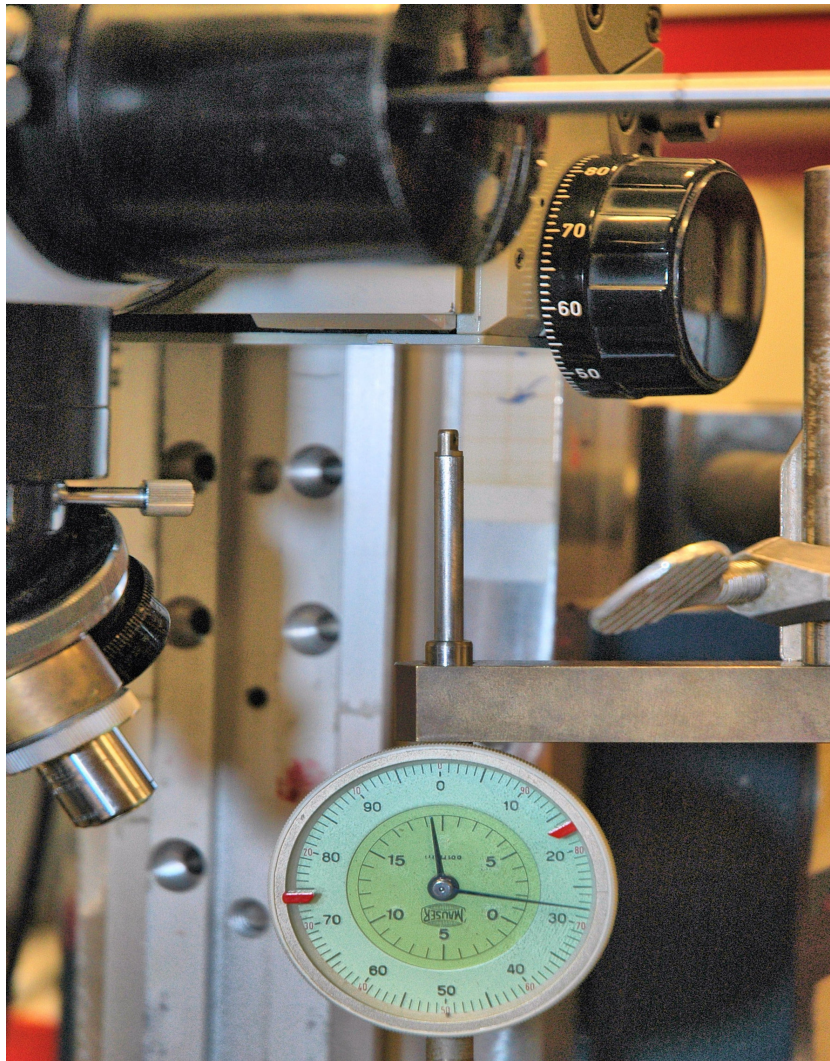
Figure 4.10: Distance measuring clock, with a resolution of 10 μ m

By programming the system to move certain amount of steps and measuring the distance traveled by the rod, a longitudinal resolution can be found as showed in final row of Table 4.2.

Table 4.2: Encoder resolution experiment, performing on the downwards movement.

Run	Counts	Distance	Resolution
1	6056	9400	1.552
2	6003	9220	1.536
3	6104	9380	1.537
4	6043	9460	1.565
5	6035	9440	1.564
6	6012	9330	1.552
7	6028	9370	1.554
8	6113	9460	1.548
9	6059	9390	1.550
10	5889	9300	1.553
11	6099	9420	1.545
12	6004	9170	1.527
13	6111	9560	1.564
14	6022	9360	1.554
15	6090	9420	1.547
16	6058	9390	1.550
17	6002	9280	1.546
18	6183	9610	1.554
19	6014	9340	1.553
20	6113	9370	1.533
AV			1.549

Finally, using the values of the mechanics present in 4.3.1.1 the steps per revolution of the encoder itself are calculated.

4.3.2   Linear Controller

In an ideal/non forced system, the control output can take any value required, and can use any variable needed to lead the system to the desired state. In real world, actuators and sensors got their own limitations and the working conditions restrict it's action, the system in interest is not the exception. In 4.3.2.1 the obtainment of the motor input limits is explained, while in 4.3.2.2 the approach for using a digital sensor is developed.

4.3.2.1   Motor Actuation

A linear control law doesn't make considerations on the system limitations, leading to undesirable behaviors such as wind up [40]. On the GRACE M-axis, the motor is forced both ways by the mass hanging in the rod and cant be powered with more than 24 V, an iterative process needs to be done to get the minimum value of input for the system to start moving. The tests consist on powering the motor starting at 20 V and stepping down

in steps of 1 V until the system stops moving, the experiment needs to be performed in both directions due the vector of gravity acting differently in the two cases. Additionally, since the control is considering friction on the motor, tests of limit values contemplate the inputs starting from repose and for keep the movement, resulting in the values displayed in Table 4.3.

Table 4.3: Minimum values for the motor calculated with a maximum value of 22.7 V for the PWM being the motor input diminished by the current limiter.

Direction	Case	PWM	Voltage
Down	Start	50	4.45
Down	Moving	40	3.56
Up	Start	130	11.57
Up	Moving	120	10.68

4.3.2.2 Speed Measurements

The lack of a speed sensor in the control loop is a non optimal situation for the implementation of the majority of control laws. Thus, the use of a dirty derivative is unavoidable [21], making the controller sensible to noise. In order to make the speed signal as suitable as possible for the closed loop, a smooth signal is imperative, consideration of mechanical, electrical and software noise sources have to be done. Due the above, tests in a data set corresponding to the motor powered at fixed voltage are performed. First, filtering algorithms including low-pass filtering and state observers are implemented to improve the signal quality, evaluating the delay in the output to preserve a representative signal as observed in Figure 4.11 and 4.12.
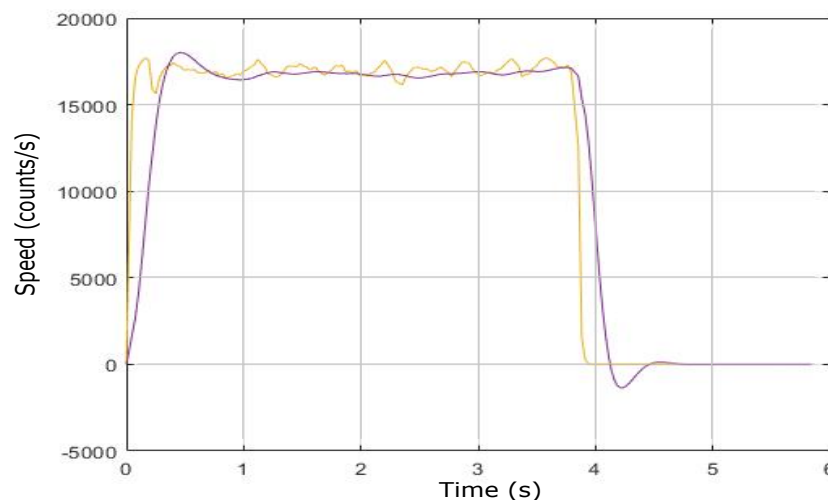
Figure 4.11: Speed measurements (counts/s) first filtering approach. The orange signal representing the raw noisy measurement and the purple the output of the low-pass filter.

The delay of the smoothed signal is near half a second making the filter not a suitable solution for incorporating the speed into a controller.
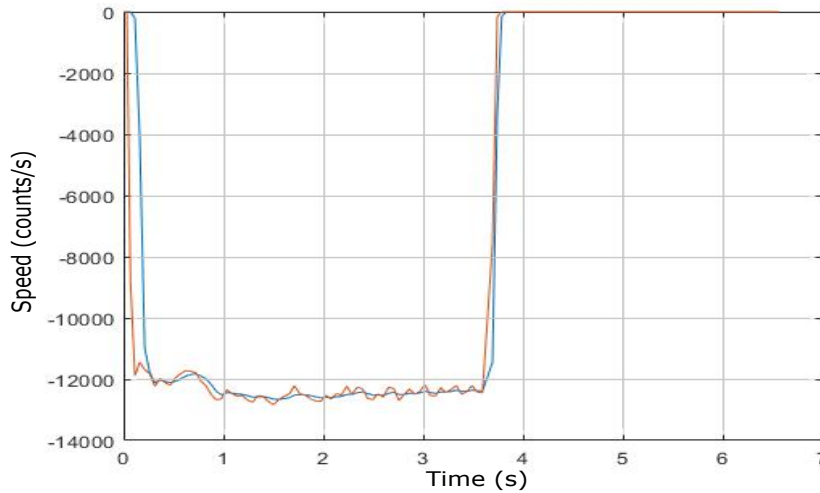
Figure 4.12: Speed measurements (counts/s) by state observer. The orange and the blue signal stand for the raw measurement and the output of the state observer respectively.

Even though, the state observer delay is small at the beginning of the movement the output takes approximately 3 seconds after the original speed to reach the repose, inducing error when close to the set point in a forthcoming controller.

Second, the measurement approach [41] is checked to ensure the best for optical encoders is used improving the signal as seen in Figure 4.13.
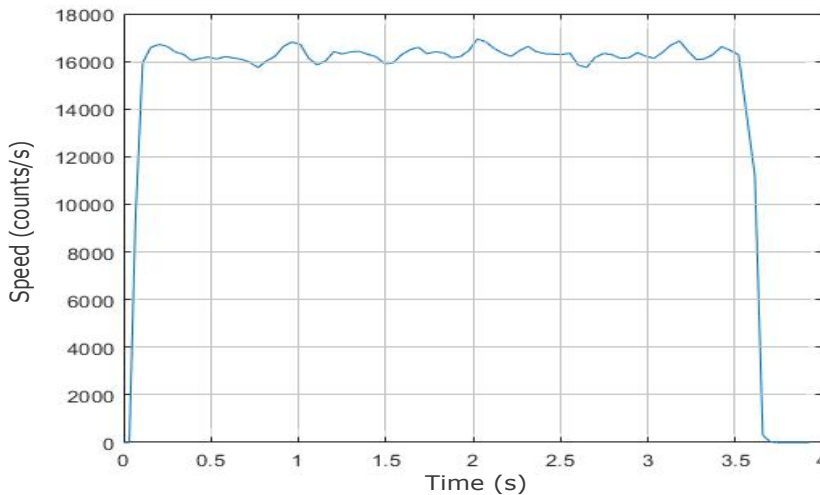
Figure 4.13: Speed measurement (counts/s) with fixated distance values.

The noise is significantly decreased respecting non fixated approach. Nonetheless, not corresponding to the linear movement it suppose to be representing.

Last, the mechanics in the setting are inspected looking for vibrations and interference in the motion of the axis, resulting in the removal of the rack in the M-axis observed in Appendix B, enhancing the speed measurement quality as observed in Figure 4.14.
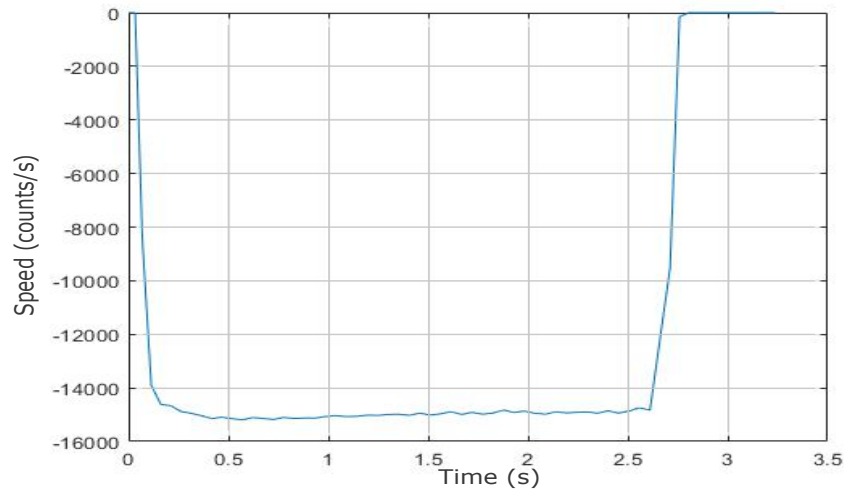
Figure 4.14: Speed measurement (counts/s) after removing the rack on the axis.

Most of the outliers of the previous attempts are eliminated, all the same, the integral of the signal is not representing the actual displacement, the previous and knowing that the time is not really an issue for the controller itself, the decision of eliminate the derivative term from the controller is taken.

4.3.3   System Model

As told in section 4.3.2.1 the motor needs different inputs depending of whether is moving or not and also regarding it's direction. To consider a range of possibilities, 4 models with voltage (V) as input and the angular position (counts) as the output, were obtained. By powering the motor at 10.68 V and 22.7, going up, and 3.56 V and 22.7 V, going down, 4 set of values were created, using the optical encoder and the Arduino. With approximately 8000 measurements per case, and using Matlab's system identification tool, the respective transfer functions (4.1), (4.2), (4.3) and (4.4), are obtained. All approximated using the state space method, expressed in the frequency domain.

$$H_u\left(s\right) = \frac{10.3977}{s^2 - 1.5528s + 0.5528}, \tag{4.1}$$

$$H_U\left(s\right) = \frac{14.6079}{s^2 - 1.5767s + 0.5769}, \tag{4.2}$$

$$H_d\left(s\right) = \frac{28.686}{s^2 - 1.6039s + 0.6040}. \tag{4.3}$$

$$H_D\left(s\right) = \frac{17.3093}{s^2 - 1.5409s + 0.5409}, \tag{4.4}$$

All four models preserve the behavior of a DC motor angular position model as explained in 2.3, the difference in the gains represent the changing behavior of the system depending on the motion.

4.3.4   Non-Linear Control Selection

As stated in 3 the second control law to be used in the GRACE is selected under four aspects previous knowledge or the availability of it, noise sensibility, factors involved and computing resources needed. In Table 4.4 the paradigms proposed to develop a more reliable solution are shown.

Table 4.4: Comparison between the the non-linear control laws proposed, where G and F stand for gravity and friction respectively

Law	Knowledge	Noise Sensibility	Factors	Computing
PD with gravity compensation	Book references [42]	High	G	Medium
port-Hamiltonian	Created in RUG	Low	G & F	High
Euler-Lagrange	Book references [22]	Low	G & F	Medium

Since the port-Hamiltonian approach was first proposed in [27] by Arjan van der Schaft, a current professor in the University of Groningen, it's implementation is known by several people in the institution, including the engineer collaborating with the laboratory. Due the above, the amount of references available for this controller are higher than the other two, the aforementioned together with consideration of gravity and friction makes this controller the one to be designed for the GRACE.

4.4   Actuator pH Model

In the present chapter a port-Hamiltonian model of the linear actuator Elero Junior 1 [35] with a mass is proposed. The model is in terms of variables and the known constants, to be suitable for any motor with a lead screw, similar to the presented in Figure 4.15. Then,the motor values and relations are shown to finally come up with the complete model.
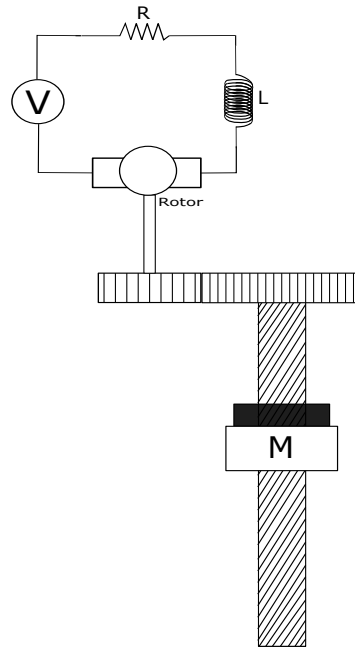
Figure 4.15: Representation of a DC motor moving a mass in a lead screw.

4.4.1 General Case

The first step is providing two differential equations that represents the electrical and mechanical behavior of a DC motor respectively. Later, the state equations are given.

$$Ri_a(t) + L\frac{di_a}{dt} = V(t) - k_m\frac{d\theta_m}{dt}, \tag{4.5}$$

$$J\frac{d^2\theta_m}{dt^2}(t) = -T(t) + k_b i_a(t) - B\frac{d\theta_m}{dt}. \tag{4.6}$$

Second, using the Hamiltonian approach [26], the energy of the system can be written in the following way,

$$H(i_a, q_m) = \frac{Li_a^2}{2} + \frac{J_m}{2}\frac{dq_m}{dt}^2, \tag{4.7}$$

being the first term of the right side of the equation the energy of the electric circuit and the second term the energy of the mechanics, both kinematic since no spring nor capacitor are part of the system. As stated in Port-Hamiltonian a new variable p_m (momenta) is defined as

$$p_m = J_m\frac{dq_m}{dt}, \tag{4.8}$$

hence, the Hamiltonian is written as

$$H(i_a, p_m) = \frac{Li_a^2}{2} + \frac{J_m^{-1}p_m^2}{2}. \tag{4.9}$$

Third, the goal is to control the system's position, becoming the aforementioned part of the model. According to the derivation of the Hamiltonian the following will be the state variables.

$$\frac{dH}{di_a} = Li_a$$

$$\frac{dH}{dp_m} = J_m^{-1}p_m \qquad (4.10)$$

$$\frac{dH}{q_m} = 0.$$

Combining (4.5), (4.6) and (4.10) a H system can be described as,

$$\begin{bmatrix} \dot{q}_m \\ \dot{p}_m \\ \dot{i}_a \end{bmatrix} = \underbrace{\begin{bmatrix} 0 & 1 & 0 \\ -1 & -B & \dfrac{k_b}{L} \\ 0 & \dfrac{-k_m}{L} & \dfrac{-R}{L^2} \end{bmatrix}}_{\overline{J}(x)-\overline{R}(x)} \begin{bmatrix} \dfrac{dH}{dq_m} \\ \dfrac{dH}{dp_m} \\ \dfrac{dH}{di_a} \end{bmatrix} + \underbrace{\begin{bmatrix} 0 \\ 0 \\ 1 \\ \dfrac{1}{L} \end{bmatrix}}_{\overline{G}(x)} V(t) + \underbrace{\begin{bmatrix} 0 \\ -1 \\ 0 \end{bmatrix}}_{\overline{B}(x)} T(t), \qquad (4.11)$$

being $\overline{J}(x)$ and $\overline{R}(x)$ respectively,

$$\overline{J}(x) = \begin{bmatrix} 0 & 1 & 0 \\ -1 & 0 & \dfrac{k_b}{L} \\ 0 & \dfrac{-k_m}{L} & 0 \end{bmatrix} \qquad (4.12)$$

$$\overline{R}(x) = \begin{bmatrix} 0 & 0 & 0 \\ 0 & B & 0 \\ 0 & 0 & \dfrac{R}{L^2} \end{bmatrix} \qquad (4.13)$$

However, the skew symmetry is not conserved on the first hand, for keeping the property is assumed the common case of a DC motor in which k_b and k_m share the same value, despite of having different units. Finally, assuming there is a lead screw with a pitch p and a diameter d_m transforming the rotation movement into a translation, is a need of a multiplying factor c to change from $\dfrac{count}{s}$ to $\dfrac{\mu m}{s}$. Therefore, the screws pitch with the amount of counts per revolution (r) will be used to get the c value. If the motor is directly connected to the screw those values would be enough to change everything using the following statements.

$$q_t = cq_m. \qquad (4.14)$$

Using (4.14) to know the displacement of the object in the lead screw, the port-Hamiltonian of linear mechanics with a DC motor becomes.

$$
\begin{bmatrix} \dot{q_t} \\ \dot{p_m} \\ \dot{i_a} \end{bmatrix} = \begin{bmatrix} 0 & c & 0 \\ -c & -B & \dfrac{k_b}{L} \\ 0 & \dfrac{-k_m}{L} & \dfrac{-R}{L^2} \end{bmatrix} \begin{bmatrix} \dfrac{dH}{dq_t} \\ \dfrac{dH}{dp_t} \\ \dfrac{dH}{di_a} \end{bmatrix} + \begin{bmatrix} 0 \\ 0 \\ \dfrac{1}{L} \end{bmatrix} V(t) + \begin{bmatrix} 0 \\ -1 \\ 0 \end{bmatrix} T(t).
\tag{4.15}
$$

4.4.2 Mass Consideration

To consider the contribution of the mass in the lead screw, on the system, the force analysis of the screw needs to be considered. In Figure 4.16 the FBD of the screw reveals two cases (lifting and lowering).
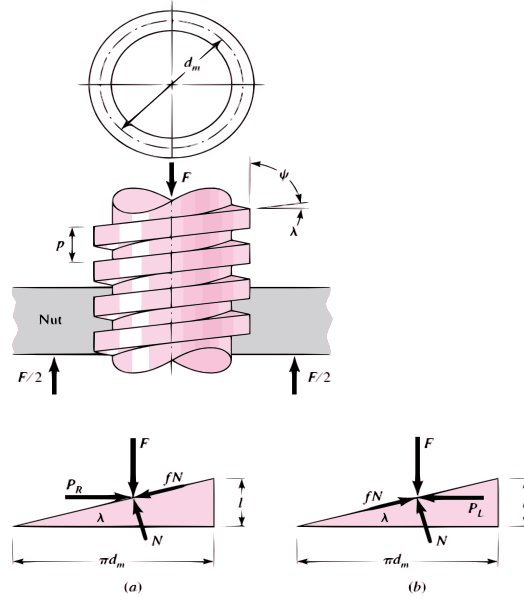
Figure 4.16: Power Screw force analysis [43]. Where F=Mg, N is the normal force, and λ, $P_{R,L}$, f are explained in Table 1.

Making use of Newton's law, the forces result in the following on the horizontal and vertical axes for the lifting,

$$
\begin{aligned}
\Sigma F_x &= P_R - N \sin \lambda - f N \cos \lambda = 0, \\
\Sigma F_y &= Mg + f N \sin \lambda - N \cos \lambda = 0,
\end{aligned}
\tag{4.16}
$$

since the normal force is not the subject of study, it can be eliminated of the equations by solving it in terms of F, and then solving for P_R.

$$
P_R = Mg \left(\frac{\sin \lambda + f \cos \lambda}{\cos \lambda - f \sin \lambda} \right),
\tag{4.17}
$$

dividing by $\cos \lambda$ and using the relation of tan, $\tan \lambda = \dfrac{p}{\pi d_m}$ the force is then:

$$P_R = Mg\left(\frac{p + d_m f \pi}{\pi d_m - fp}\right). \tag{4.18}$$

Using the same process the lowering case goes from (4.19) to (4.20),

$$\begin{aligned} \Sigma F_x &= -P_L - N \sin \lambda + fN \cos \lambda = 0, \\ \Sigma F_y &= Mg - fN \sin \lambda - N \cos \lambda = 0, \end{aligned} \tag{4.19}$$

$$P_L = Mg\left(\frac{d_m f \pi - p}{fp + \pi d_m}\right). \tag{4.20}$$

Revealing the equations above the values of the external force opposing the movement in the screw plain, depending mainly on the direction of the movement. The aforementioned forces are caused by the self-locking property of the lead screws, only true if $f > \tan \lambda$ [43]. The system does not moves when the motor is not powered, confirming the lack of potential energy in the system even though the linear system is on the y axis. The mathematical expressions in (4.18), (4.20) are forces in the plain of the screw, which means that the actual torques actuating in the rotational system still need to be found. Since the screw plain analyzed consist in the thread at it's medium diameter, the torques affecting the motors are,

$$T_R = \frac{d_m P_R}{2}, \tag{4.21}$$

$$T_L = \frac{d_m P_L}{2}. \tag{4.22}$$

In order to express the external force of the model T(t) changes to become dependant of the speed, telling this last one the direction. Having two cases, suddenly changing from one to another at speed equal zero, the approximate model of the external force is,

$$T_{ls}(p_m) = \frac{1}{2}(T_R + T_L) + \frac{1}{2}(T_R - T_L)\frac{p_m - c_g}{\sqrt{a_f + (p_m - c_g)^2}}, \tag{4.23}$$

with a_f a value close to z and c_g the inflection point desired. Knowing what is the expression behind the force, the system can be expressed as the following,

$$\begin{bmatrix} \dot{q}_t \\ \dot{p}_m \\ \dot{i}_a \end{bmatrix} = \begin{bmatrix} 0 & c & 0 \\ -c & -B & \dfrac{k_b}{L} \\ 0 & \dfrac{-k_m}{L} & \dfrac{-R}{L^2} \end{bmatrix} \begin{bmatrix} \dfrac{dH}{dq_t} \\ \dfrac{dH}{dp_t} \\ \dfrac{dH}{di_a} \end{bmatrix} + \begin{bmatrix} 0 \\ 0 \\ \dfrac{1}{L} \end{bmatrix} V(t) + \begin{bmatrix} 0 \\ -1 \\ 0 \end{bmatrix} T(p_m). \tag{4.24}$$

4.4.3   Elero Junior 1 model

The system in (4.24) is presented with the assumption of having the screw directly con-
nected with the motor, but in the current case there is gearing between the motor, the
encoder and the screw as seen in the Figure 4.17.
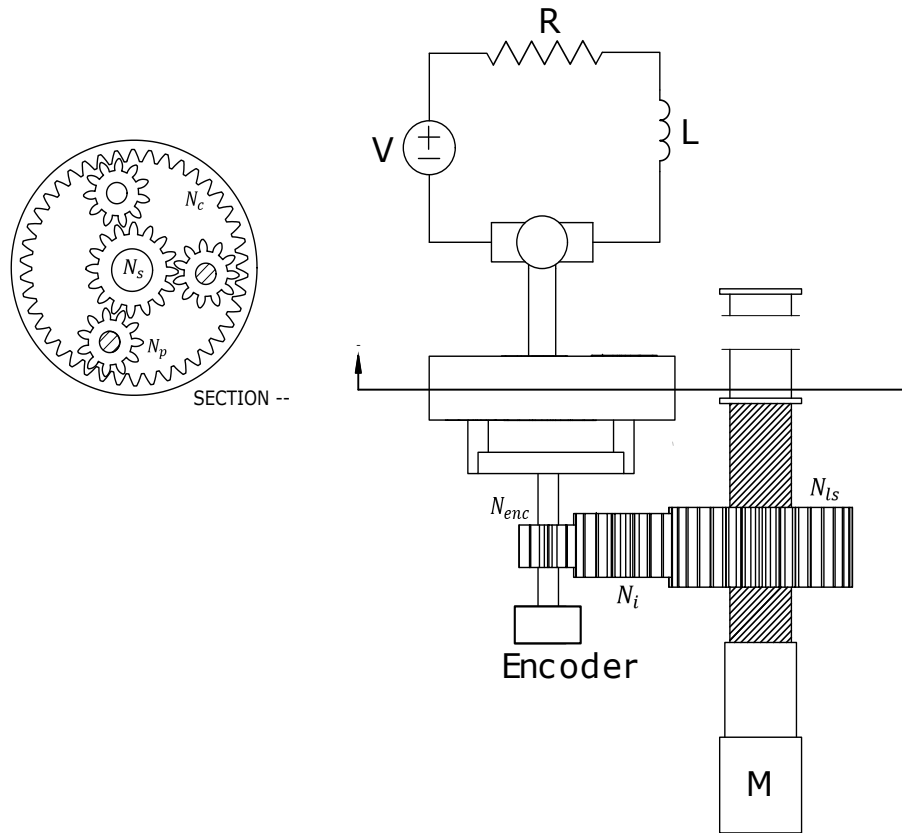
Figure 4.17: Elero real arrangement

Knowing the amount of the teeth (presented in Table 1 is just needed to specify each
arrangement to transform the motion values. First, there is a solar gearing with the
motor as the input, and the output on the encoder shaft, being the motor on the sun gear
and the second driven by the three planets. Considering the crown as the output and it's
speed equal zero, the planet gears as the intermediate and the sun as the input, the e
(gear train value) can be written as,

$$e = \frac{\omega_c - \omega_p}{\omega_s - \omega_p} = \frac{0 - \omega_p}{\omega_s - \omega_p}, \tag{4.25}$$

$$e = \frac{n_{in}}{n_{out}} = \frac{16}{41}, \tag{4.26}$$

resulting in an expression of the encoder's shaft speed in terms of the motor's;

$$\omega_{enc} = \frac{-16\omega_m}{25} \tag{4.27}$$

Then, from the encoder to the screw a regular gear coupling is done, being the encoder the input and the lead screw the output,

$$\omega_{in} n_{in} = \omega_{out} n_{out}, \tag{4.28}$$

$$\omega_{ls} = \frac{9}{34} \omega_{enc} \tag{4.29}$$

With all the conversion factors for the rotational motion the only left is the torque values. Based on the power equation (4.30) for the rotating systems

$$P = \omega T, \tag{4.30}$$

considering energy conservation on the gearing and applying the conversions on the velocity, the following are calculated,

$$T_{enc} = \frac{25 T_m}{16}, \tag{4.31}$$

$$T_{ls} = \frac{34 T_{enc}}{9}. \tag{4.32}$$

The way the system measures the angle is by an optical encoder with a resolution of r samples per revolution, which is connected by the relation showed in (4.29) to the screw which dimensions are showed in Table 1, can result in a $c = 1.55 \frac{\mu m}{count}$ (confirmed later by the manufacturer) or in $c = 252.6 \frac{\mu m}{rad}$. Incorporating the new values and considering that the values are not measured directly into the motor, the Port-Hamiltonian becomes the following:

$$\begin{bmatrix} \dot{q}_t \\ \dot{p}_m \\ \dot{i}_a \end{bmatrix} = \begin{bmatrix} 0 & c & 0 \\ -c & -B & \frac{25 k_b}{16L} \\ 0 & \frac{-25 k_m}{16L} & \frac{-R}{L^2} \end{bmatrix} \begin{bmatrix} \frac{dH}{dq_t} \\ \frac{dH}{dp_t} \\ \frac{dH}{di_a} \end{bmatrix} + \begin{bmatrix} 0 \\ 0 \\ \frac{1}{L} \end{bmatrix} V(t) + \begin{bmatrix} 0 \\ \frac{-9}{34} \\ 0 \end{bmatrix} T_{ls}(p_m). \tag{4.33}$$

By experimentation the values of the PWM to move the system are obtained in 4.3.2.1. Using the torque constant of the motor seen in [44], the torque used in each operation can be obtained.

$$T_m = k_t i = \begin{cases} 1.55 Ncm & Down \ 19\% \ PWM \\ 3.38 Ncm & UP \ 51\% \ PWM. \end{cases} \tag{4.34}$$

Using the expressions in (4.31) and (4.32), the torque generated by the motor can be moved to the lead screw resulting into:

$$T_{ls} = \begin{cases} 9.15 Ncm & T_L \\ 19.89 Ncm & T_R \end{cases} \tag{4.35}$$

Assuming a friction coefficient between aluminum and steel showed in Table 1, the apparent mass of the system can be obtained from both (4.21) and (4.22), getting both similar results in (4.36).

$$M_{L/R} = \begin{cases} 5.67 kg \\ 5.14 kg. \end{cases} \tag{4.36}$$

The difference between values can be attributed to non considered friction on the rail or energy lost during the current limitation.

Chapter 5

Results and Discussion

In the current Chapter the final product of the design process regarding the hardware is explained and analyzed. Additionally, experimental results relevant for the work done are discussed, including the performance of the finished system.

5.1 Hardware

In Chapter 4 the improvements respect to [4] were presented individually, nonetheless, the coalescence of all components into the circuit is the final result of the design process for the M axis controller and is shown on Appendix A.
As seen in the schematic, the dedicated pins for SPI communication, serial ports, and interruptions are not used if not necessary. The AC-DC converter is the power input to the motor and the DC-DC converters, assuring the necessary power always will be available.

The circuit designed fulfill the needs of the controllers and accomplishes the minimum use of dedicated I/O for the system to incorporate new features. Additionally, the voltage dissipation changed from 2,3 V when going up and 1,8 when going down, to a constant 1,2 V. The above makes the system more efficient in terms of, the pins used and maximum voltage exploit respectively. The manual positioning mode made by a potentiometer mapping the speed of the motor, is not suitable for precision work, resulting just in a way of reducing the distance traveled by the motor once the automatic control is activated. The above is one of the aspects which can be improved by changing/adding new components to the present design, such as high precision ADCs or an optical encoder as an input.

The hardware used ensures the safety for the user and GRACE, incorporating a security measures in the resistor arrangement to prevent the motor, and the circuit itself from burning. Furthermore, by grounding the case shown in Figure 5.1 with the circuit inside, and eliminating heating components to avoid short circuits and burning for the user.

Figure 5.1: Final box with the controller

5.2   Graphic User Interface

After a process of feedback done with the final users of the tool, the final GUI with the features wanted are showed in the Figure 5.2. The system shows the position in both counts and μm and the LED controller is done by a slider with a range of values from 0 to 255 to fit exactly the PWM, the absolute setting button drives the motor to it's top end to have an absolute position on the system.
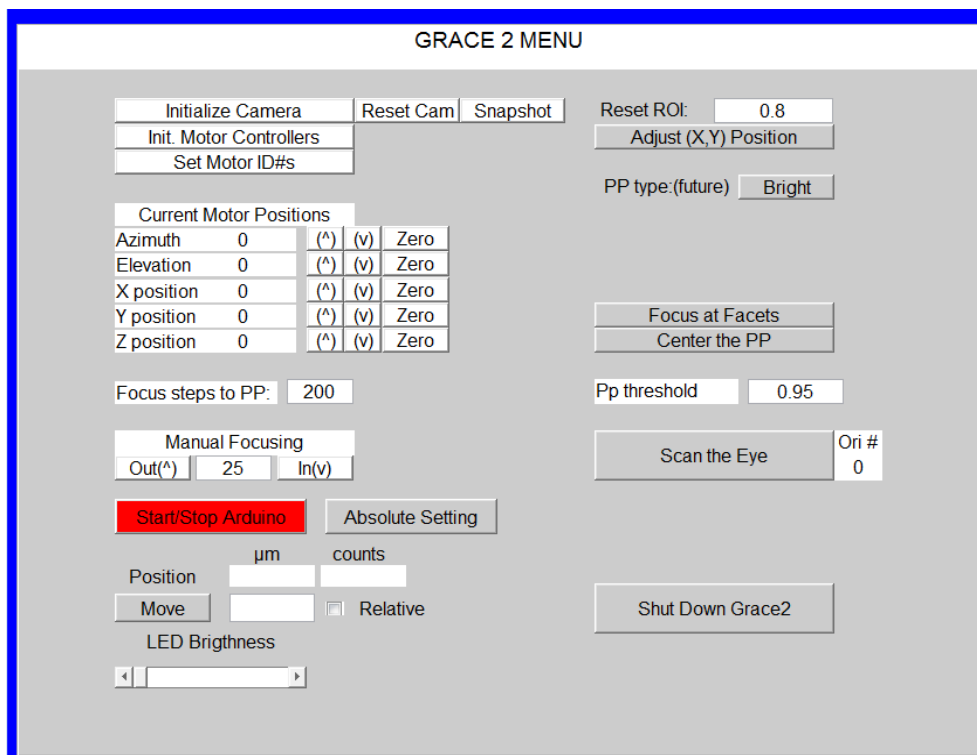

Figure 5.2: GRACE updated GUI, including the telemicroscope control situated in the bottom left. The color of the Start/Stop button tells whether the GUI is communicating with the Arduino or not.

The software used in the GUI proves to be receiving data and sending instructions with an asynchronous communication being able to keep the user updated with the system status and controlling the LED and the motor hardware at the same time as the remaining 5 DOF of GRACE.

The display of the data in Figure 5.2 seems to be explicit enough to the user, showing the value of the position in both units. Additionally, the controller can be used in absolute and relative position thanks to the check box and the absolute button, to specify the set point and the initialization frames.

Since the GUI is only intended to be used when either of the controllers is on automatic, the buttons of it are useless when this is not the case. However, if the user doesn't check the switches of the box presented in 5.1, there is no way of tell whether the system is on manual or the communication is not working properly, making the GUI not aware of the state of the whole system.

5.3   Arduino Software

The Arduino script created shows an efficient develop in managing the tasks given, controlling the two output while making use of the I2C and the decoding system for the screen and the PC communication respectively. The software manages to tell the direction of the system by looking at the pin out values for the motor control, however, with the presence of the channel A in the encoder this task would consume less resources and improve the accuracy.

The automatic and manual mode identification, the LED control, the screen refresh and the PC communication are recurrent functions called in all levels of the logic in order to break the current task, regulate the brightness and update the data at any moment. In the case of the first one, the use of interrupts could have incorporated a more sophisticated solution in exchange of the only interrupt pins left. The receiving of data from the PC is bounded to the automatic modes, meaning that if none of the controllers is set on automatic, the Arduino only ignores the incoming data, and then cleans the serial port to eliminate noise from the channel.

5.4   Experimental Results

5.4.1   PID controller

The experimentation done with the speed measurements reveal a poor quality signal, not appropriate to use in the closed loop. The Arduino can filter the speed calculations using a state observer, transforming the mentioned in an smooth input for the controller sacrificing processing time resulting in a delayed signal that is not suited for sudden

changes in the motion.

Since the model doesn't behave as any of the presented cases in 2.4.1.4, the values were stated empirically. After several attempts of tuning, based on the solely simulation of the four models presented in 4.3.3 individually, the parameters of the controller are a set of values obtained using the response (4.1) and (4.4). The result is a PI controller transforming into a P depending on the value of the error as shown in expression (5.1).

$$
C\left(t\right) = \begin{cases} 6.3416x10^{-3}e + \dfrac{1}{159.79} \int edt & e \geqslant 10000 \ counts \\ 2.374x10^{-3}e & < 10000 \ counts. \end{cases} \tag{5.1}
$$

Set point tests are done to retrieve the settling time and the stable state error, in Figures 5.3 and 5.4 the aforementioned values are marked plots.
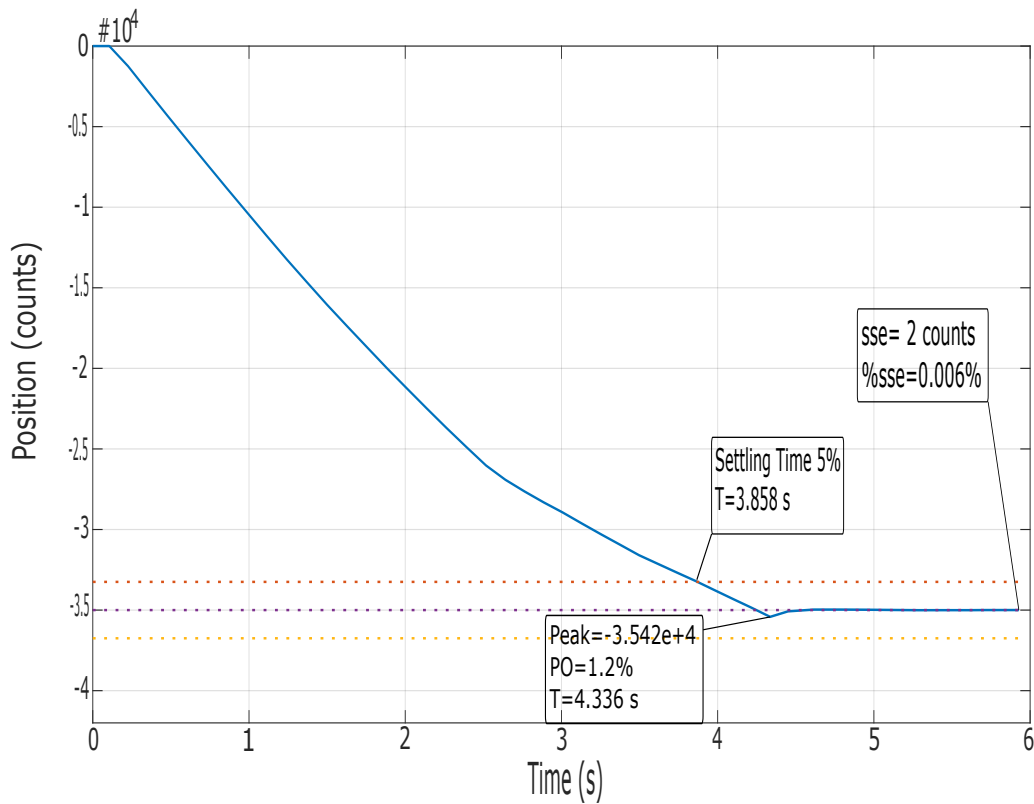

Figure 5.3: Test of the linear controller for the actuator going up to a set point 35000 counts upper from the start position
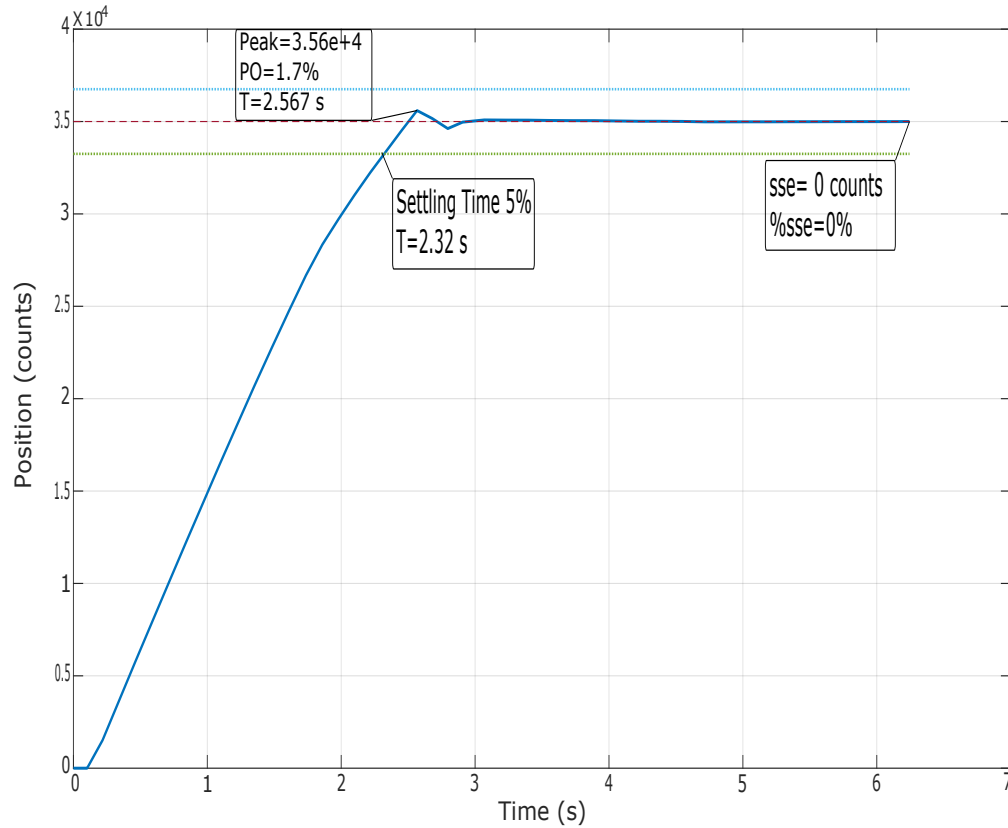
Figure 5.4: Test of the linear controller for the actuator going up to a set point 35000 counts downer from the start position

The PID ended up as a PI control with two different set of values for its constants transforming into a proportional control when the error is low. The lack of a derivative gain is attributed to the noise the speed calculation introduces to the system and the damping the derivative control adds to the closed loop, resulting in a weak control output. Moreover, the elimination of the integral in the final result is related to the oscillations the integrating action incorporate to the behavior, being it undesirable due the lash the mechanics could present.

According to the rotational sensor the desired position is reached, however the measure is made in an intermediate stage of the actuator, to validate the accuracy of the rod position the analog mechanical sensor used in 4.3.1.2 is employed, where the controller is set at the same point in different runs, resulting in the set of values in Table 5.1.

Table 5.1: Position set point validation, comparing the final position error of the system (RSSE) with for the same measured by the controller (SSE), and getting the final value of error after applying the magnification of the optics (RSSEO) for the real system all expressed in μm.

Run	RSSE	SSE	RSSEO
1	-210	3	-8.4
2	80	1	3.2
3	20	2	0.8
4	-170	2	-6.8
5	-80	-3	-3.2
6	-20	3	-0.8
7	-70	3	-2.8
8	110	3	4.4
9	-20	-3	-0.8
10	100	-3	4
AV	-26	0.2	-1.04

The linear controller used have proven to accomplish the requirements of the solution needed in the majority of the cases, with the help of the limit winding done by experimentation 4.3.2.1, which change depending on the sign of the speed. The set point is reached according to the optical encoder, but far from good when the validation is done. This is attributed to two main reasons, first, the mechanical arrangement between the sensor and the final state present backlash, creating a dead zone when the motor is starting and stopping it's movement [45]. Second, the malfunctioning of the channels B and O, which tell the direction and the time a full turn is completed respectively, forced a software based direction consideration. The aforementioned, provokes the system to not detect if the position is oscillating on the dead zones of the mechanics. However, the optics of the system dictates an overall displacement 25 times smaller than the sensed with the encoder, resulting in a successful range of stable state error on 8 out of 10 of the runs.

The use of a second sensor for the linear motion is the most evident solution, if the desired stable state error is to be guaranteed 100% times. By modeling a spring on the gearing to justify the difference between the rotation and the displacement, a real state of the rod can be obtained. Even though, the previous suggestion, implies changes on the pH model created in 4.4, since the use of a spring adds potential energy to the system.

5.4.2   Control with only position measurements

After the system presented in 4.4 the control designed was based on the explained in 2.6.1 and using the equation developed in [26], resulting in the following energy shaping and dynamical extension:

$$\overline{V}_d = \frac{1}{2}k_p\left(q_m - q_{md}\right)^2 + \frac{1}{2}k_c\left(q_m - q_{md} - q_c\right)^2, \tag{5.2}$$

with the first term on the right side being the energy shaping and the second the extension. Having the original system no potential energy, a new equation can be defined as desired if it follows the other criteria explained in (2.31) and (2.32), by the energy shaping the dynamics of the extension are obtained.

$$\frac{\partial \overline{V}_d}{\partial q_c} = -k_c(q_m - q_{md} - q_c), \tag{5.3}$$

$$\dot{q}_c = -R_c^{-1}\frac{\partial \overline{V}_d}{\partial q_c}. \tag{5.4}$$

with trial and error, the values of the system are tuned obtaining the values of Table 5.2.

Table 5.2: Port-Hamiltonian Values for the controller

Constant	Value
k_p	2
k_c	10
R_c	5

Finally obtaining the controller seen in (5.5).

$$u = -k_p(q_m - q_{md}) - k_c(q_c), \tag{5.5}$$

simulations are run for the system going both ways to a set point 100 radians, equivalent to 25261 μm, from the origin, the results are seen in Figures 5.5 and 5.6.
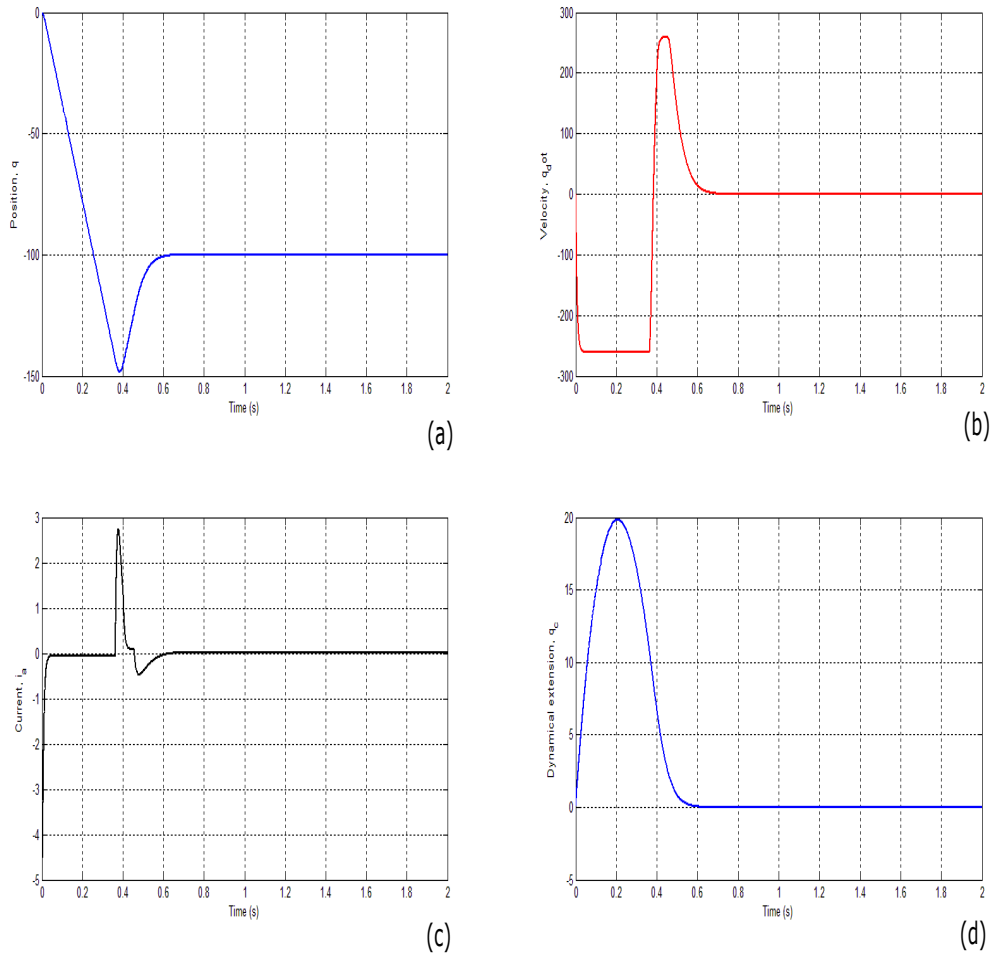
Figure 5.5: Control with only position measurements performance on the Elero Junior actuator moving upwards. The graphics show the behavior of the position (a), velocity (b), current (c) and the virtual state (d).
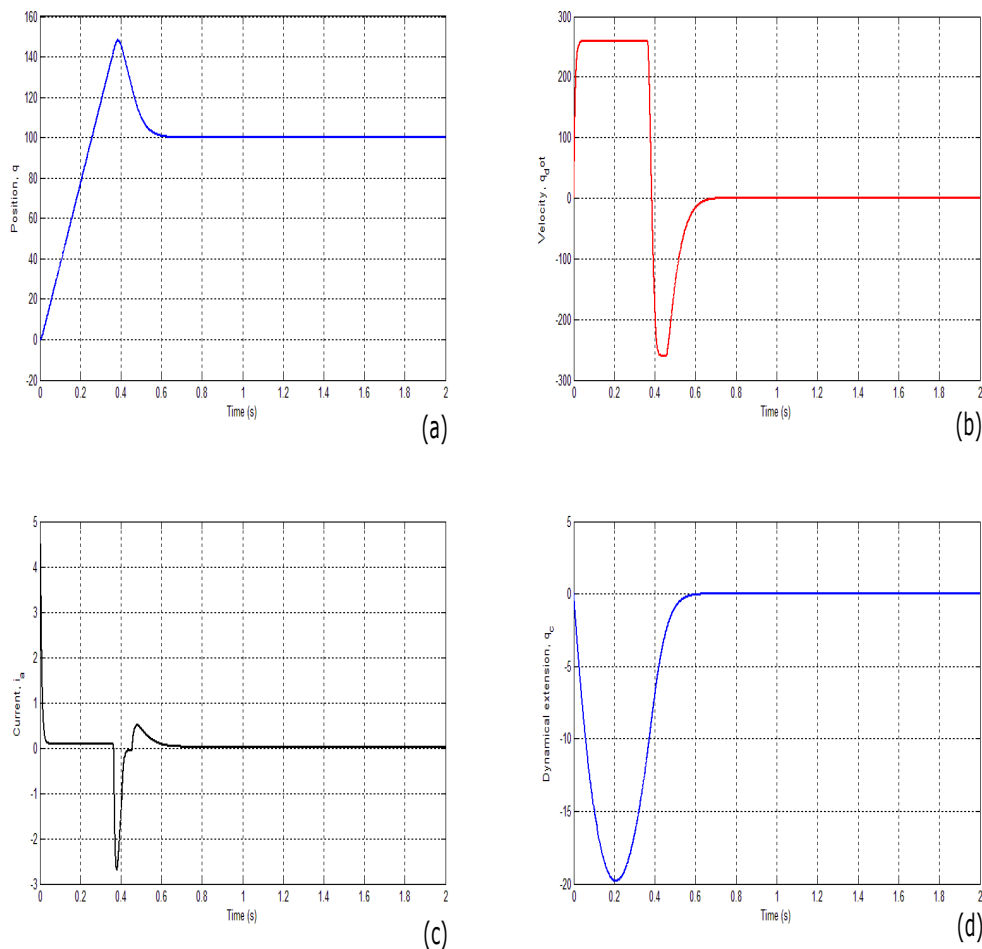
Figure 5.6: Control with only position measurements performance on the Elero Junior actuator moving downwards. The graphics show the behavior of the position (a), velocity (b), current (c) and the virtual state (d).

The systems new potential energy is bounded to the old one, since before the extension the only energy present on the arrangement is kinetic, any potential shaping can be proposed, as long as it satisfy the requirements presented in 2.6.1. The simulations show a forced system stabilized by using the dynamic of the extension introducing what in terms of the controller design is the damping needed, however, the dynamics of the extension are based only on the position of the original system, creating an integral value when the virtual position is obtained. The model of the system created in 4.4 uses a force disturbance change it's value depending on the direction, making the only position measurements partial since the only value needed is the sign of the motion. The current plot (c), shows inrush currents bigger than the permitted by the limiter on the circuit for the actuator to reach the set point. Giving the above the suggestion of changing the powering system of the motor to get better results with either controller.

Chapter 6

Conclusions

The design and implementation of the hardware creates a more efficient current limitation and a user friendly for the manual mode of the controllers which protects both the user and the system due the aspects presented in 5.1.

The software satisfy the requirements for the control of both brightness and position, being the system capable of dealing with both at the same time no matter the operating mode. The new GUI makes possible the full automatic control of GRACE using the PC only, showing the state of the 6 DOF at the same time.

The optical encoder used in the rotational section of the actuator is not enough to measure the state of the rod, the malfunctioning of channels A and O contribute to the bad performance of the sensor, luring the system to measure the encoder improperly when this is moved by anything but the voltage input, such as the lash or inertia.

The motor manual mode is suitable for raw positioning, nonetheless getting real precision out of it is nearly impossible using just a mapping of the potentiometer position to control the speed of the motion.

The linear controller developed couldn't be tuned using any standard method due the order of the system and changing nature of the system presented in 4.3.3.The desired performance of the aforementioned is achieved 80% of the cases according to the verification done with a mechanical measure in the position of the rod.

Neither the PID nor the pH controller can deal with the lash of the system since the encoder is placed before the mechanics making the lash dead zones untraceable.

Chapter 7

Recommendations

The implementation of the linear control law revealed that no control law can bring the system to the desired value, due the mechanics in the middle of the encoder and the rod, in order to improve the accuracy on the GRACE M-axis, different and non exclusive measures are considered:

- Implementing a specialized motor driver with a circuit suitable to withstand the high inrush currents can enhance the motor actuation.

- The manufacturing of a new mechanical setting using anti lashing design on the components to eliminate the uncertainty generated by the couplings.

- Incorporate a new full functioning encoder, eliminating the direction assumption of the software. Therefore, detecting the system's direction at all times.

- Adding an extra position sensor on the rod, generating two different position states could result in a more realistic model for both the control laws.

- The change of the DC motor for more powerful actuator or the addition of a fine tuning position control made with a stepper or servo motor.

- To accomplish a precise manual motor control the implementation of a trajectory tracking with one of the components mentioned in 5.1 is suggested.

The GUI doesn't tell the user whether the circuit is on automatic or manual mode, in order to make it fool proof an alarm needs to be implemented.
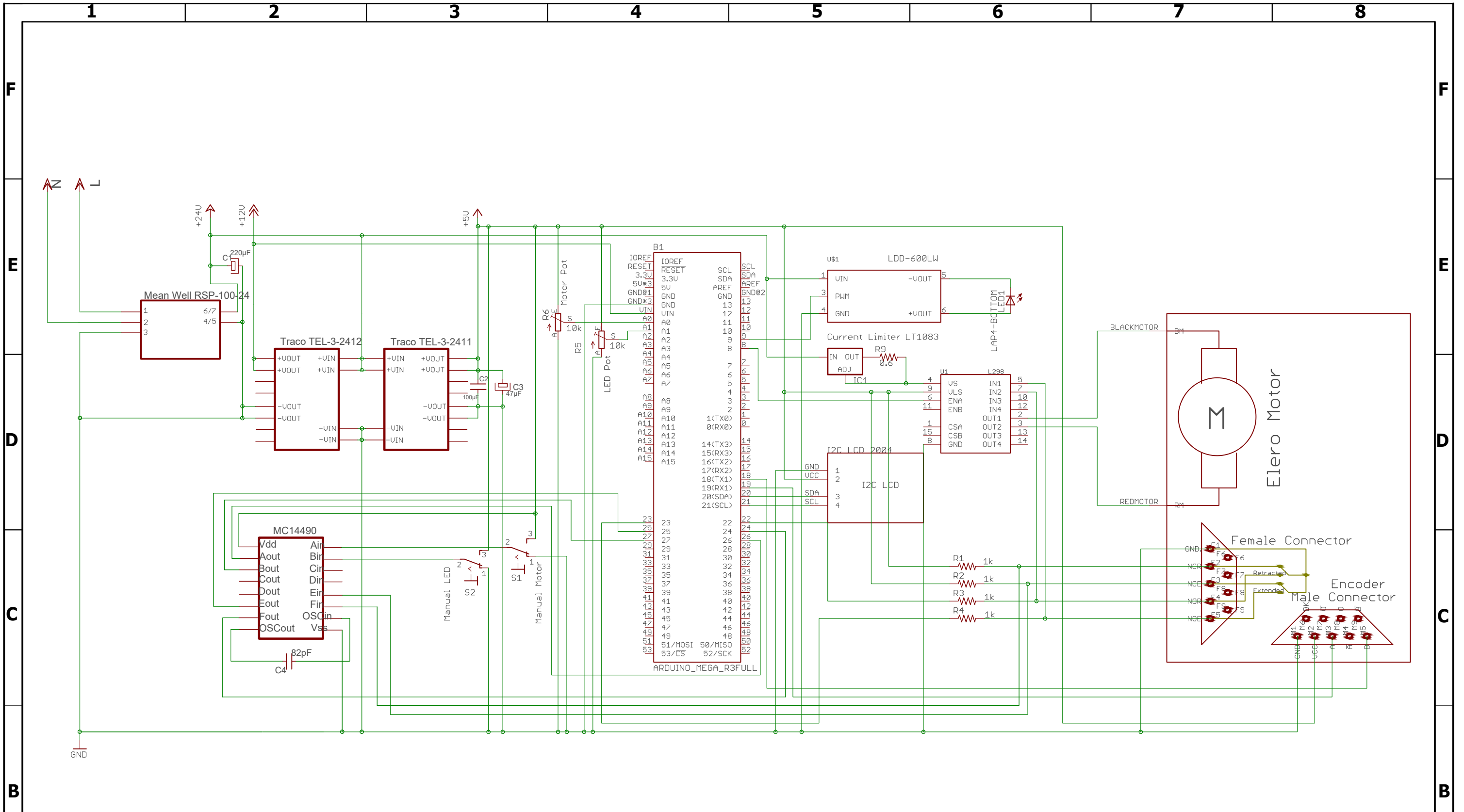
Bibliography

[1] T. Spanier, "The design and implementation of the full actuation for the five dof 3d robotic scanner," July 2015.

[2] M. Guzman-Fonseca, "Design and implementation of an autofocusing algorithm for the goniometric robotic apparatus for compound eyes," September 2017.

[3] K. K. Sahu, "Automated image feature identification for motorized mapping of insect eyes," August 2017.

[4] D. Reinders, T. Steinfort, Y. Sinnige, W. Berendschot, and J. de Poel, "Automated light intensity and camera positioning for the goniometric robotic apparatus for compound eyes," June 2018.

[5] D. Stavenga, "Reflections on colourful ommatidia of butterfly eyes," *The Journal of Experimental Biology*, vol. 205, pp. 1077–1085, 2002.

[6] W. Retana-Calvo, "Design and implementation of a 6 degrees of freedom controller for the grace system," November 2016.

[7] M. van der Horst, "Design of an angular position measurement system and controller for a 3d robotic scanner," August 2016.

[8] J. A. Vargas-Delgado, "An image stiching algorithm for compound vision research," August 2016.

[9] D. Stavenga, "Pseudopupils of compound eyes," in *Comparative Physiology and Evolution of Vision in Invertebrates* (H. Autrum, ed.), ch. 7, pp. 357–439, Berlin: Springer, 1979.

[10] Z. Kan, J. Yei Hwan, M. Solomon, S. Jung-Hun, K. Munhi, M. Hongyi, Z. Han, X. Zhenyang, Z. Weidong, G. Shaoqin, and M. Zhenqiang, "Origami silicon optoelectronics for hemispherical electronic eye systems," *Nature Communications*, vol. 1782, no. 1AB, pp. 1–8, 2017.

[11] D. Floreano, R. Pericet-Camara, S. Viollet, F. Rfflier, A. Bruckner, R. Leitel, W. Buss, M. Menouni, F. Expert, R. Juston, M. K. Dobrzynski, G. L'Eplattenier, F. Recktenwald, H. Mallot, and N. Franceschini, "Miniature curved artificial compound eyes," *PNAS*, vol. 110, no. 23, pp. 9267–9272, 2013.

[12] A. Snyder, D. Stavenga, and S. Laghlin, "Spatial information capacity of compound eyes," *Journal of Comparative Physiology*, vol. 116, pp. 183–207, 1977.

[13] D. Stavenga and K. Arikawa, "Evolution of color and vision of butterflies," *Arthropod Structure Development*, pp. 307–318, 2006.

[14] LED Hoge Spanning, *LED with Heatsink 3W*. CH-LED-3W-45MIL-D. 2018.

[15] T. Instruments, "Pid theory explained," November 2018. [Online; posted 19-November-2018].

[16] ECE, "Closed loop speed control of a DC motor," 2017.

[17] K. Ogata, *Modern Control Engineering*. Pearson, 2010.

[18] M. Shahrokhi and A. Zomorrodi, "Comparison of pid controller tuning methods,"

[19] ElectronicsHub, "Pid theory explained," December 2015. [Online; posted 10-December-2015].

[20] I. I. of Techonology of Kharagpur, "Controller tuning." "https://nptel.ac.in/courses/108105063/pdf/L-13(SS)%20(IA&C)%20((EE)NPTEL).pdf".

[21] R. Ortega, A. Loria, P. Nicklasson, and H. Sira-Ramirez, *Passivity-based Control of Euler-Lagrange Systems: Mechanical, Electrical and Electromechanical Applications*. Springer-Verlag London, 1998.

[22] C. Byrnes, A. Isidori, and J. Willem, "Passivity, feedback equivalence, and the global stabilization of minimum phase nonlinear systems," *Transactions on automatic control*, vol. 36, no. 11, pp. 1228–1240, 1991.

[23] D. Morin, *Introductory Classical Mechanics*. Cambridge, 2007.

[24] A. Wolski, "Review of hamiltonian mechanics." https://www.cockcroft.ac.uk/wp-content/uploads/2014/12/wolski-1.pdf, 2012.

[25] M. Muñoz-Arias, *Energy-based control design for mechanical systems*. RUG, 2015.

[26] D. Dirksz, *Robust energy-and power-based control design*. RUG, 2011.

[27] B. M. Maschke and A. J. van der Schaft, "Port-controlled hamiltonian systems: Modelling origins and system theoretic properties," *Symposium on Nonlinear Control Systems*, pp. 90–95, 1992.

[28] J. C M Van Der Burg, R. Ortega, J. Scherpen, J. Acosta, and H. Siguerdidjane, "An experimental application of total energy shaping control: Stabilization of the inverted pendulum on a cart in the presence of friction," *2007 European Control Conference, ECC 2007*, 07 2007.

[29] R. Ortega and M. Spong, "Stabilization of underactuated mechanical systems via interconnection and damping assignment," *IEEE Transaction on Automatic Control,* pp. 1218–1233, 2000.

[30] G. Blankenstein, R. Ortega, and A. Van Der Schaft, "The matching conditions of controlled lagrangians and ida-passivity based control," *International Journal of Control,* vol. 75, pp. 645–665, 2002.

[31] D. Dirksz, J. M. A. Scherpen, and R. Ortega, "Interconnection and damping assignment passivity-based control for port-hamiltonian mechanical systems with only position measurements," *IEEE Conference on Decision and Control,* pp. 4957–4962, 2008.

[32] G. Pahl, *Engineering Design: A systematic Approach.* Springer, 2005.

[33] K. Hurst, *Engineering Design Principles.* Elsevier, 1999.

[34] Wiki, "I2c lcd2004." http://wiki.sunfounder.cc/index.php?title=I2C_LCD2004.

[35] Elero, "Linear actuator junior." https://www.elero-linear.com/en/products/linear-actuators/junior-1/, 2015.

[36] ON Semiconductor, *Hex Contact Bounce Eliminator.* MC14490. Rev. 10. 2013.

[37] Traco Power, *DC/DC Converters.* Tel 3 Series. Rev 6. 2018.

[38] Standa, "Stepper dc motor controller." http://www.standa.lt/products/catalog/motorised_positio 525.

[39] A. S. Dijkstra, "Grace graphical user interface," June 2018.

[40] A. Bemporad, "Anti-windup techniques." http://cse.lab.imtlucca.it/~bemporad/teaching/ac/pdf/AC2-09-AntiWindup.pdf, 2010.

[41] J. Sachs, "How to estimate encoder velocity without making stupid mistakes." https://www.embeddedrelated.com/showarticle/158.php, 2012.

[42] R. Kelly, *Control of Robot Manipulators in Joint Space.* Springer, 2005.

[43] R. Budynas and J. Keith Nis, *Mechanical Engineering, Shigley's Mechanical Engineering Design.* McGraw-Hill, 2006.

[44] Dunkerenmotoren, *DC Motors.* GR42X20. Rev. 2. 2017.

[45] Designatronics, "How backlash affects gears, elements of metric gear technology." http://www.sdp-si.com/resources/elements-of-metric-gear-technology/page7.php.

Appendix A

LED/Motor Control Circuit

LED/Motor Control Circuit

Appendix B

GRACE's Rack for manual movement

Figure B.1: Rack on the rail of GRACE system, with a different resolution than the lead screw, it was a cause of interference.